OPTIMIZATION OF TWO-PHOTON EXCITED FLUORESCENCE ENHANCEMENT BETWEEN TUNABLE AND BROADBAND FEMTOSECOND LASER PULSE EXCITATIONS

A Dissertation

by

CHAO WANG

Submitted to the Office of Graduate Studies of
Texas A&M University
in partial fulfillment of the requirements for the degree of

DOCTOR OF PHILOSOPHY

December 2011

Major Subject: Biomedical Engineering

Optimization of Two-photon Excited Fluorescence Enhancement between Tunable and Broadband Femtosecond Laser Pulse Excitations

Copyright 2011 Chao Wang

OPTIMIZATION OF TWO-PHOTON EXCITED FLUORESCENCE ENHANCEMENT BETWEEN TUNABLE AND BROADBAND FEMTOSECOND LASER PULSE EXCITATIONS

A Dissertation

by

CHAO WANG

Submitted to the Office of Graduate Studies of
Texas A&M University
in partial fulfillment of the requirements for the degree of

DOCTOR OF PHILOSOPHY

Approved by:

Chair of Committee,	Alvin T. Yeh
Committee Members,	George W. Kattawar
	Kenith Meissner
	Michael McShane
Head of Department,	Gerard L. Coté

December 2011

Major Subject: Biomedical Engineering

ABSTRACT

Optimization of Two-photon Excited Fluorescence Enhancement between Tunable and Broadband Femtosecond Laser Pulse Excitations. (December 2011)

Chao Wang, B.A., Xiamen University

M.S., Shanghai Jiao Tong University

Chair of Advisory Committee: Dr. Alvin Yeh

This project explores optimization of two-photon excited fluorescence (TPEF) enhancement between tunable narrowband and un-tuned broadband femtosecond (fs) laser pulse excitations for two-photon microscopy (TPM). The research is conducted preliminarily in time domain and comprehensively in frequency domain to understand the physics behind TPEF enhancement by un-tuned sub-10 fs nearly transform-limited pulse (TLP) versus tunable 140 fs pulse. The preliminary study on inverse proportionality of TPEF yield to fs-pulse duration delimits a general lower-bound to narrowband fs-pulse regime (pulse duration > 40 fs) with assumption of dye-molecule frequency invariant response. Deviations from this inverse proportionality in broadband fs-pulse regime (pulse duration < 40 fs) highlights dye-molecule frequency variant response, necessity of group delay dispersion (GDD) compensation, and broadband TLP for TPEF enhancement.

The follow-up comparative study is made on un-tuned sub-10 fs TLP versus tunable 140 fs pulse excitations using three dye-phantoms (Indo-1, FITC, and TRITC)

representative of fluorescent probes with similar TPEF characteristics. The integrated experimental system, with custom-designed GDD compensation, dispersion-less laser-beam expanding and focusing, and compound-lens for efficient fluorescence collection with good spectral resolution, ensures accurate TPEF measurements. Differentiated TPEF enhancements of Indo-1 (1.6), FITC (6.7), and TRITC (5.2) proportionally agree with calculated ones due to the overlap of fs-pulse second harmonic (SH) power spectrum with dye-molecule two-photon excitation (TPE) spectrum. Physically speaking, with broadband sub-10 fs TLP readily involved in both degenerate ($\nu_1 = \nu_2$) and non-degenerate ($\nu_1 \neq \nu_2$) two-photon absorption (TPA), this un-tuned ultrashort fs-pulse excitation simultaneously allows for more accessibility to TPA-associated final states and diversely promotes population of thus excited dye-molecules with the three dye-phantoms. Under environmental influences (mutual quenching through one-photon absorption(s) and solvent effect), multicolor TPEF enhancement observed from a mixture of the three dyes shows promise of sub-10 fs TLP as simultaneous excitation for multiple-dye labeled samples in contrast to compromised excitation with narrowband fs-pulse tuning. Both single- and multicolor TPEF enhancements clarify tradeoff between tunability of narrowband fs-pulse and un-tuned broadband fs-pulse excitations, being instructive to further considerations on optimization of TPEF enhancement by strategic utilization of broadband fs-pulse for better performance of TPM.

ACKNOWLEDGEMENTS

I would like to thank my committee chair, Dr. Alvin T. Yeh, and my committee members, Dr. George W. Kattawar, Dr. Kenith Meissner, and Dr. Mike McShane, for their guidance and support throughout the course of this research. While writing this dissertation, I recalled with great pleasure academic communications with Dr. A. V. Sokolov and Dr. George W. Kattawar during our one-year association at the weekly multi-group meeting in the Department of Physics at TAMU, where I gained invaluable experience and background knowledge on femtosecond laser pulses that played an important role in my research. I am deeply grateful to Dr. Kenith Meissner for his advice on usage of manually tunable Ti:Sapphire laser and triple-grating spectrograph and helpful discussions on one-photon absorption and solvent effects. I wish to express my thanks to Dr. Michael McShane and his graduate students, Brad Collier, Jason Roberts, and Dustin Ritter, to whom I owe a debt of gratitude for their assistance with measurements of one-photon absorption and fluorescence. Thanks also go to Dr. Brian E. Applegate who arranged for the use of the software-controlled tunable Ti:Sapphire laser in his laboratory. I acknowledge that Dr. Stan Vitha and Dr. Andreas Holzenburg in the Microscopy and Imaging Center at TAMU arranged for the construction of the two-photon microscope system and use of the un-tune sub-10 fs Ti:Sapphire laser from which I gained invaluable professional experience. I also want to extend my gratitude to the National Science Foundation (Faculty Early Career Development Award and CEBT-1033660) for support on this research project.

TABLE OF CONTENTS

LIST OF FIGURES

FIGURE Page

FIGURE Page

LIST OF TABLES

CHAPTER I

INTRODUCTION: THE BACKGROUND AND SIGNIFICANCE OF RESEARCH

Two-photon microscopy (TPM) [1], a modality of nonlinear optical microscopy, has brought many new research opportunities to biological and medical sciences and is becoming a routine microscopy tool for molecular imaging in laboratories [2]. TPM makes use of fluorescence signals generated *in situ* inside thick bio-samples for imaging [3]. Physically speaking, visible fluorescence emission occurs concurrently with relaxation of fluorophore molecules priorly excited by near-infrared (NIR) laser pulses through the third-order non-parametric process of two-photon absorption (TPA) [4], which could be summarized as Two-Photon Excited Fluorescence (TPEF). Due to very low TPA cross sections of fluorophores currently in use ($\sim 10^{-50}\ \frac{cm^4 s}{photon^2}$ [4], or simply $\sim 10^{-50} GM = 10^{-50}\ \frac{cm^4 s}{photon}$ [2]), routine operation of TPM requires ultrashort NIR laser pulses of $\sim$100 femtosecond (fs) durations tightly focused with high numerical aperture (N.A.) objective lens. Readily satisfied by state-of-the-art Ti:Sapphire laser systems [5], these stringent conditions for TPM operation effectively localize TPEF generation to the focal volume of femto-liters and greatly suppress out-of-focus fluorescence background and photobleaching, enabling three-dimensional imaging to probe endogenous and exogenous fluorophores in thick bio-samples. In practice, imaging depth is limited by

---

This dissertation follows the style of Journal of Optical Society of America B.

bio-sample turbidity associated with scattering properties [6] and by signal-to-background ratio (SBR) [7], i.e., ratio of TPEF *in situ* to out-of-focus fluorescence background. In addition to excellent optical sectioning, TPM has other advantages over confocal one-photon fluorescence microscopy [8]. First, NIR laser pulse falls in much weaker one-photon absorption and scattering window of bio-samples [6], which allows larger penetration depths and significantly reduces thermal effect on the sample. Second, large spectral separation between NIR laser pulse and fluorescence emission facilitates TPEF detection by spectral filtering.

Fundamentally, time-averaged TPEF yield $\langle F(t)\rangle$ versus time-averaged power of laser excitation $\langle P_{laser}(t)\rangle$ (tuned to a central wavelength $\lambda_{laser} = \frac{2\pi c}{\omega_{laser}}$)[1] follows the square-law dependence [4,9], i.e.,

$$\langle F(t)\rangle = \frac{1}{2} g \phi \eta_2 C \sigma^{TPA}_{S_0 \to S_f}(\omega_{laser}) \frac{8n\langle P_{laser}(t)\rangle^2}{\pi \lambda_{laser}} . \quad (1)$$

Both $\langle F(t)\rangle$ and $\langle P_{laser}(t)\rangle$ are quantities to be acquired in TPEF measurements. The g-factor ($= \frac{g_p}{f\tau_p}$) describes the 2nd-order temporal coherence degree of the fs-pulse excitation including pulse-repetition-rate f, pulse duration τ_p, and pulse shape factor g_p [10,11]. ϕ is fluorescence collection efficiency of a specific experimental setup. η_2 is TPEF quantum efficiency of a specific fluorescent dye, commonly assumed to be the same as that of one-photon excited fluorescence (OPEF) η_1 for the same dye-phantom

[1] c is light speed in free space.

[9]. C is molar concentration of the fluorescent dye-phantom. n is ensemble-averaged refractive index of the sample medium. Eq. (1) holds true as the rule of thumb for affirming TPEF provided that all the relevant parameters remain unchanged during TPEF measurements at a tuned laser wavelength. Without loss of generality, absolute TPA cross section [4,12] $\sigma_{S_0 \to S_f}^{TPA}(\omega_{laser})$ of the dye-molecule, being laser frequency dependent and as sum over all the excited states (SOS), could be simplified as

$$\sigma_{S_0 \to S_f}^{TPA}(\omega_{laser}) \propto \left. \frac{M_{01}^2 M_{1f}^2}{(\Delta E_{01} - \hbar\omega)^2} \right|_{(\Delta E_{01} - \hbar\omega) >> \Gamma_{damp}}, \quad (2)$$

with the assumptions that the first excited singlet state S_1 of the dye-molecule be the dominant intermediate state and that narrowband fs-pulse excitation frequency ω_{laser} be far from resonance with the dye-molecule, i.e., $(\Delta E_{01} - \hbar\omega_{laser}) >> \Gamma_{damp}$. Γ_{damp} is the damping factor [4] for the $S_0 \rightarrow S_1$ transition of energy gap ΔE_{01} (S_0 is the ground singlet state). M_{01} and M_{1f} are transition dipole moments of $S_0 \rightarrow S_1$ and $S_1 \rightarrow S_f$ (TPA-associated final state). Eq. (1) as well as Eq. (2) is the master formula governing the experimental work and theoretical analysis on optimization of TPEF herein.

Ever since its advent, improvements on TPM have centered on its two assets, i.e., good optical sectioning and large-depth imaging, which are related to TPEF enhancement one way or the other and SBR of images. Since amplified narrowband fs-pulses may improve SBR to some extent [7], TPEF enhancement mostly resorts to ~100 fs laser pulse excitations tuned to a wavelength where a specific fluorescent probe (either organic or synthesized [12-14]) exhibits the largest TPA cross section (refer to Eq. (2)).

This optimization of TPEF enhancement with narrowband fs-pulse tuning originates in the fact that absolute TPA cross section $\sigma^{TPA}_{S_0 \to S_f}(\omega_{laser})$ of a fluorescent probe is excitation wavelength/frequency dependent. With narrowband fs-pulse tuning, absolute TPA cross sections of a specific dye-phantom versus tuned laser wavelengths can be obtained from measurements of action TPA cross section ($\eta_2 \sigma^{TPA}_{S_0 \to S_f}(\omega_{laser})$) [9] assuming that η_2 be known. This is equivalent to TPEF measurements with a specific dye-phantom excited at the same power level by narrowband fs-pulse stepwise central wavelength tuning over a designated range. The accordingly obtained two-photon excitation (TPE) spectrum refers to the TPEF yields versus the narrowband fs-pulse tuned wavelengths, which illustrates that the TPEF yields are proportional to the absolute TPA cross sections versus the narrowband fs-pulse tuned wavelengths (Eq. (1)). In principle, TPE spectrum of a specific dye-phantom could be used to determine the optimal wavelength of the narrowband fs-pulse for TPEF enhancement since the TPE spectrum peak position corresponds to this optimal wavelength for the largest TPA cross section of the dye-molecule.

Technical advances in state-of-the-art Ti:Sapphire lasers provide opportunities to explore new methods for optimization of TPEF enhancement with TPM. Strategic utilization of coherence properties of fs-pulse excitation is being used to formulate efficient excitation schemes for TPEF enhancements [15-19] by various techniques of pulse shaping spectrally and /or temporally. Generally speaking, TPEF signals can be effectively enhanced by decreasing pulse duration down to sub-10 fs owing to its higher peak power than that of ~100 fs pulse from tunable Ti:Sapphire lasers. This method for

TPEF enhancement was mostly inspired by the inverse proportionality of TPEF yield $\langle F(t) \rangle$ versus pulse duration τ_p formulated by the $g = \frac{g_p}{f\tau_p}$ factor in Eq. (1) [9] provided that the pulse shape factor g_p remain unchanged as the transform-limited pulse duration declines. In one previous study [9], a prism pair instead of BK7 plate(s) was used to introduce spectral phase chirp for τ_p variation without considering group delay dispersion (GDD) compensation with regard to the objective lens used for narrowband fs-pulse focusing and TPEF collection. This neglect of GDD compensation could not ensure the transform-limited pulse as the pulse duration declined, leading to 7% deviation from the inverse proportionality slope -1 of $\langle F(t) \rangle$ versus τ_p in the range of 90 fs ~ 230 fs for Indo-1 phantom. More significant deviation from -1 slope happened with τ_p decreased below 90 fs. GDD compensation was still ignored in the follow-up study [20] on the inverse proportionality with the fs-pulse duration declining until 12 fs, which led to noticeable deviation ($\tau_p^{-0.85}$) from the slope -1 of $\langle F(t) \rangle$ versus τ_p because the chirp effect on fs-pulse could not be eliminated with the prism pair and BK7 plate(s) to deal with both fs-pulse duration variation and GDD compensation. In addition, higher-order dispersion by the prism glass also contributes to the overall chirp effect. Enlightened by the multiphoton intrapulse interference phase scan (MIIPS) method capable of achieving 2nd- and higher-order dispersion compensation for selective excitation of different cell organelles with TPM [21], re-study of the inverse proportionality of $\langle F(t) \rangle$ versus τ_p was made with common organic dyes (FITC, TRITC, and Texas-red), two Ti:Sapphire lasers (Mira Coherent and Synergy

Femtosecond), chirp mirror pair together with fused glass wedges and BK7 plate(s) for optimal GDD compensation, and with intra-cavity slit and interference bandpass filters for pulse duration variation [22]. Calculations of the two-photon transition probabilities with measured data for each dye phantom were conducted according to the phenomenologically introduced formula [23], i.e.,

$$\Gamma_{TPA} = \int_0^\infty \gamma(\omega) \left| \int_0^\infty A\left(\tfrac{\omega}{2} + \Omega\right) A\left(\tfrac{\omega}{2} - \Omega\right) d\Omega \right|^2 d\omega, \tag{3}$$

where $\hbar\omega$ is the transition energy, $\gamma(\omega)$ is TPE spectrum of the dye-phantom, and the squared integral refers to the fs-pulse second harmonic (SH) power spectrum converted from the measured laser spectrum. The calculations were carried out by using the TPE spectrum obtained from measured TPEF yields of the dye-phantoms and SH power spectrum of laser and Gaussian-shaped fs-pulses according to [24]

$$E(\omega) = E_0(\omega - \omega_c) \exp\left[i \frac{\Phi''}{2} (\omega - \omega_c)^2 \right], \tag{4}$$

where ω_c is the pulse central frequency and Φ'' designates GDD effect on the Gaussian shaped fs-pulse. All the data calculated by Eq. (3) and Eq. (4) are shown together in Fig. 1 to explore how two-photon transition probabilities follow the general trends established with the Gaussian shaped pulse. The non-identical profiles with Gaussian (points) and experimental (circles) pulse spectra are due to differences in fs-pulse shape [15]. For narrowband fs-pulse of durations $T_p \geq 40\,fs$, two-photon transition probabilities should follow the $\frac{1}{T_p}$ relationship for all the three dye-phantoms. This is the narrowband fs-pulse regime where excitation schemes with TPM are currently

selected. Deviation from the $\frac{1}{T_p}$ relationship becomes evident with all the three dye-phantoms as the fs-pulse duration decreases below 40 fs into the broadband fs-pulse

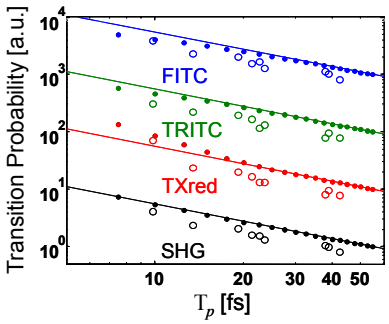

Fig. 1. Calculated two-photon transition probabilities versus pulse duration for FITC, TRITC, Texas-red, and SHG using Gaussian shaped (points) and experimental (circles) pulse spectra. Solid lines of -1 slope are shown for reference [22].

regime. This is because of the wide overlap of TPE spectrum of a specific dye-molecule with SH power spectrum of the broadband fs-pulse in contrast to nearly uniform and narrow overlap in the narrowband fs-pulse regime. These characteristic deviations are dye-molecule dependent, i.e., The two-photon transition probabilities with FITC and TRITC phantoms curves downward while that with Texas-red upward. The fs-pulse SH power spectrum adheres to the $\frac{1}{T_p}$ relationship over the entire range of pulse duration variation, which corresponds to the theoretical assumption of dye-molecule frequency

invariant response. The above-made analysis on measured data summarized in Fig. 1 implies that the degree of overlap between the TPE spectrum of dye-molecule and fs-pulse SH power spectrum should be the key for optimization of TPEF enhancement. And the best candidate for the latter (fs-pulse SH power spectrum) would be that of the transform-limited pulse (TLP). This hypothesis is verified by good agreement between the calculated and measured TPEF signals both versus the TLP duration (Fig. 2).

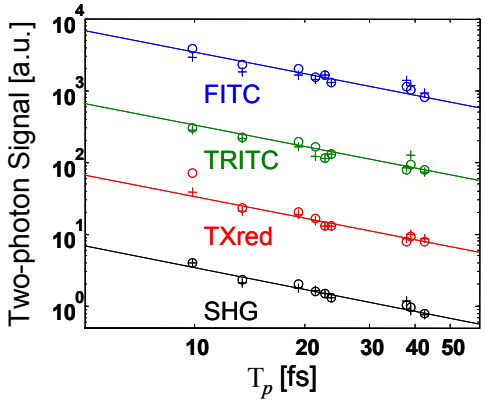

Fig. 2. Calculated (circles) and measured TPEF signals with FITC, TRITC, Texas-red, and SHG (crosses), all versus transform-limited pulse duration [22].

In contrast to the ideal case of transform-limited pulses, noticeable deviation from the $\frac{1}{T_p}$ relation of $\langle F(t) \rangle$ versus T_p with Texas-red phantom excited by linearly chirped and transform-limited pulses is shown in Fig. 3, whose trends can be said of other dye-phantoms or SHG under the same experimental conditions.

However, this strategy for optimization of TPEF enhancement based on the inverse proportionality of TPEF yield versus fs-pulse duration seems to be faced with a dilemma, i.e., tunability of narrowband fs-pulse versus un-tuned broadband mode-locked

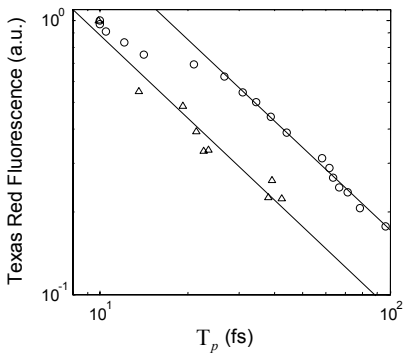

Fig. 3. Fluorescence signals with Texas-red excited by chirped (circles) and transform-limited pulses (triangles) with solid lines of -1 slope for reference [22].

fs-pulse. Abided by the Fourier transform relation, ultrashort fs-pulses can be achieved with Kerr lens mode-locking by involving broader pulse spectrum. As the duration is declining toward sub-10 fs and below, the pulse spectral full-width at half-maximum (FWHM) would span larger than 100 nm, close to the gain bandwidth of Ti:Sapphire [25], which makes wavelength tuning of ultrashort fs-pulse infeasible. Consequently, central wavelength of the un-tuned broadband fs-pulse is likely detuned from the dye-molecule TPE spectrum peak position. For those fluorophores whose TPE spectrum peak positions are distributed throughout the gain bandwidth of Ti:Sapphire, lack of

central wavelength tunability seemingly suggests a disadvantage in the use of un-tuned broadband fs-pulses for optimization of TPEF enhancement. Clarification on this tradeoff by quantifying TPEF enhancement *via* TPEF measurements with tunable narrowband and un-tuned broadband fs-pulse excitations would help understand the mechanism behind TPEF enhancement one way or the other.

This research project is motivated by the desire to explore possible ways for optimization of TPEF enhancement between tunable narrowband fs-pulse and un-tuned broadband fs-pulse. In this comparative study, TPEF enhancements by tunable narrowband versus un-tuned broadband fs-pulse excitation are comprehensively investigated through single- and multicolor TPEF measurements. These two excitation schemes refer to the un-tuned sub-10 fs TLP centered at 792 nm and the 140 fs pulse tuned from 700 nm to 900 nm at 10 nm increment. The major aspects of the novelty in this experimental study are stated as follows. In reference to the experiences gained from the preliminary study on the inverse proportionality of TPEF yield $\langle F(t) \rangle$ versus pulse duration τ_p, importance of GDD compensation for maintaining transform-limited fs-pulse excitation is highly stressed with special attention given to experimental setup designs to ensure delivery of nearly transform-limited pulse (TLP) *in situ* (at the focal spot of the dye-phantom center). In order to make a comprehensive study on single- and multicolor TPEF enhancements, a custom-designed spectral detection system for fluorescence collection is assembled and well calibrated for accurate TPEF measurements because good spectral resolution is required with a triple-grating spectrograph as the detector rather than a photomultiplier tube (PMT) used in

conventional TPEF spectroscopy [9]. In order to acquire a good understanding of TPEF enhancements with the two excitation schemes, three organic dyes of distinct TPEF characteristics are carefully selected to represent fluorescent probes with similar properties, i.e., the fluorescent dyes with their TPE spectrum peak positions (corresponding to their largest TPA cross sections) located about the high-frequency wing (for Indo-1), the spectral peak (for FITC), and low-frequency wing (for TRITC) of the sub-10 fs TLP spectrum. Then, differentiated TPEF enhancements could be readily observed from the three dye-phantoms whose TPE spectra overlap with the fs-pulse SH power spectrum in their distinct ways. Expectedly, observations made and conclusions drawn from these case studies could be generalized to evaluation of two-photon excitation capability of the broadband fs-pulse excitation with regard to the fs-pulse SH power spectrum. On the other hand, compromised excitation schemes for multiple-dye labeled bio-samples by narrowband fs-pulse tuning currently with TPM could not be satisfactory for *in vivo* molecular imaging when good temporal and spectral resolution of multicolor TPEF signals are desired. The empirically determined “optimal” wavelength of a compromised excitation may give misleading information about distribution of fluorophore molecules in the sample, which makes image processing and biological interpretations difficult. In addition, environmental influences on fluorescent probes in a multiple-dye labeled bio-sample further diminish discernability of the measured multicolor TPEF profiles, which complicates the interpretation of the multicolor TPEF images as well. Therefore, optimization of multicolor TPEF enhancement between tunable and broadband un-tuned fs-pulse excitations should take into account

environmental influences on fluorescent probes and incorporate with multi-channel spectral detection. This research project focuses on fundamental issues about optimization of TPEF enhancement and clarifies some ambiguities relevant to this major theme. Practically, exploration of new methods for optimization of TPEF enhancement aims at (1) enhancing TPEF signals *in situ* with improved SBR and (2) simultaneous excitation of multiple-dye labeled bio-samples to facilitate imaging processing and biological interpretation of multicolor TPEF images. The former would further improve optical sectioning (i.e., spatial resolution of images) at large imaging depths, providing new opportunities for imaging applications with TPM. The latter potentially would be a better alternative to the compromised excitation scheme for multiple-dye labeled bio-samples under environmental influences in hope of producing spectral cross-talk free images from which appropriate interpretations with biological significance could be made.

CHAPTER II

MATERIALS AND METHODOLOGY

The integrated experimental setup (Fig. 4A) for this comparative study consists of three units: (1) two excitation schemes with group delay dispersion (GDD) compensation (Fig. 4B) for delivering the sub-10 fs TLP; (2) dispersion-less laser-beam expanding and focusing with parabolic mirrors; and (3) TPEF collection with a custom-designed compound-lens coupled to a spectrograph. This experimental system design ensures delivery of the sub-10 fs TLP *in situ* (i.e., at the focal spot of the phantom center), high

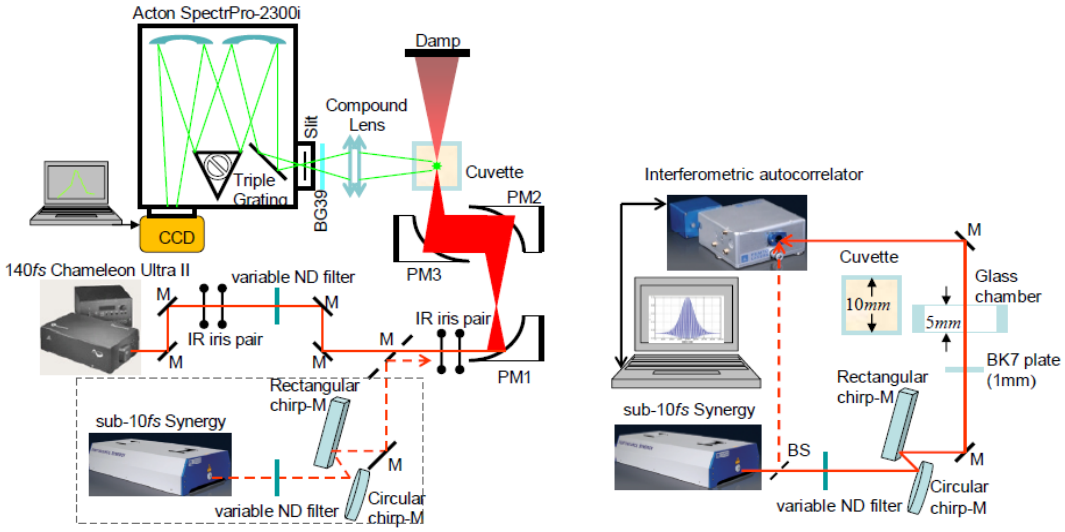

(A) (B)

Fig. 4. (A) Experimental configuration for TPEF measurement; (B) optimization of GDD compensation.

efficiency of fluorescence collection, and good spectral resolution for accurate TPEF measurements.

2.1 Two excitation schemes

A software-controlled tunable Ti:Sapphire laser (pulse duration 140 fs, pulse-repetition-rate 80 MHz, horizontal linearly polarized, Chameleon Ultra II, Coherent) is used for TPEF measurements over the tuning range from 700 nm to 900 nm at 10 nm increment. This tuning range well approximates the spectral full-width at tenth-maximum (FWTM) (~ 190 nm) of the sub-10 fs mode-locked pulses from the un-tuned Ti:Sapphire laser (central-wavelength 792 nm, FWHM ~ 130 nm, pulse-repetition-rate 75 MHz, Synergy^{TM} PRO, horizontal linearly polarized FEMTOLASERS). A variable neutral density (ND) filter (spectral window 380 nm ~ 1200 nm, Thorlabs) is used for laser power adjustment. The accumulative GDD of cuvette (1.25mm-thick optical-glass-window, 10.0 mm path-length, 23/G/10, Starna Cells), dye-phantom, and ND filter is assumed negligible for the 140 fs pulses with the spectral FWHM less than 9 nm [5,22].

Compared to narrowband fs-pulses, broadband fs-pulses of duration down to sub-10 fs are much more vulnerable to group velocity dispersion (GVD) [26,27] when propagated over a distance L in an optically dispersive material. The spectral phase of the fs-pulse electric field can be expressed as

$$\Phi(\omega) = -k(\omega)L\,, \tag{5}$$

whose propagation constant $k(\omega) = \frac{2\pi\nu}{c} n(\nu) = \frac{\omega}{c} n(\omega)$ is ω dependent. After the Taylor series expansion until the 3rd-term, Eq. (5) transforms into the truncated phase factor

(over the propagation distance L in the dispersive medium)

$$\Phi(\omega) = \Phi(\omega_c) + \frac{\partial \Phi}{\partial \omega}(\omega - \omega_c) + \frac{1}{2}\frac{\partial^2 \Phi}{\partial \omega^2}(\omega - \omega_c)^2, \tag{6}$$

where ω_c is the central frequency of the fs-pulse. Eq. (5) can also transform into its truncated propagation constant (over per unit propagation distance in the dispersive medium)

$$k(\omega) = k(\omega_c) + \frac{\partial k}{\partial \omega}(\omega - \omega_c) + \frac{1}{2}\frac{\partial^2 k}{\partial \omega^2}(\omega - \omega_c)^2, \tag{7}$$

which is related to Eq. (6) by $\Phi(\omega) = -k(\omega)L$. The phase velocity of the spectral component ω can be expressed as

$$v_{ph}(\omega) = \frac{c}{n(\omega)} = \frac{\omega}{k(\omega)}. \tag{8}$$

The 1st-, 2nd- and 3rd-term in Eq. (7) respectively define the propagation constant $k(\omega_c)$ of the fs-pulse central frequency component, the group velocity of a spectral component ω of the fs-pulse

$$\left.\frac{\partial k}{\partial \omega}\right|_{\omega} = \frac{1}{v_g(\omega)} = \frac{n(\omega) + \omega \frac{dn}{d\omega}}{c}, \tag{9}$$

and the GVD of that spectral component ω

$$\left.\frac{\partial^2 k}{\partial \omega^2}\right|_{\omega} = \frac{d}{d\omega}\left[\frac{1}{v_g(\omega)}\right]_{\omega} = \frac{1}{c}\left(2\frac{dn}{d\omega} + \omega\frac{d^2 n}{d\omega^2}\right). \tag{10}$$

In practice, the group delay $\tau_g(\omega) = \frac{L}{v_g(\omega)}$ for a spectral component ω over a

propagation distance L is used instead of the group velocity $v_g(\omega)$. Accordingly, the group delay dispersion (GDD) is defined as

$$\Delta\tau_g(\omega) = \tau_g(\omega) - \tau_g(\omega_c) = \frac{\partial \tau_g}{\partial \omega}(\omega - \omega_c)$$

$$= \frac{\partial\left(v_g^{-1}\right)}{\partial \omega}(\omega - \omega_c)L = \frac{\partial^2 k}{\partial \omega^2}\bigg|_{\omega} (\omega - \omega_c)L$$

$$= \left(2\frac{dn}{d\omega} + \omega\frac{d^2 n}{d\omega^2}\right)\frac{(\omega - \omega_c)L}{c}, \qquad (11)$$

which refers to the time-lag of a spectral component ω with respect to the central frequency component ω_c when they co-propagate inside the fs-pulse envelope over a distance L in a dispersive medium (or, through a thickness L of an optical element). The 1st- and 2nd-order material dispersion terms ($\frac{dn}{d\omega}$ and $\frac{d^2 n}{d\omega^2}$) in Eq. (11) manifests the origin of GDD, which implies GDD compensation by neutralizing normal dispersion from the optical elements involved in TPEF measurements with specially fabricated optical components of anomalous dispersive properties. With deliberately designed GDD compensation, nearly TLP *in situ* with minimized phase variations could be achievable, which is essential for the sub-10 fs pulse whose broad bandwidth spans an order of magnitude larger than that of the narrowband 140 fs pulse. Otherwise, appreciable GDD accumulated by optical elements involved in TPEF measurements will cause temporal broadening [28] as well as peak power drop to the incident sub-10 fs mode-locked pulse, so seriously that the fs-pulse characteristics *in situ* become far different from intrinsic properties of the mode-locked sub-10 fs directly from the un-

tuned laser.

Among the three types of optical components (grating, prism, and chirp-mirror) typically used for GDD compensation, a pair of chirp-mirrors is optimally selected from those available in the laboratory to compensate for the positive GDD caused by cuvette, dye-phantom, and ND filter. This GDD compensation is designed on the following considerations. The grating-pair is not an option because it takes up excessively large space for installation and requires delicate alignment. The prism-pair, though more compact, will introduce higher-order dispersion terms due to their own glass thickness, which compromises the GDD compensation with considerable residual dispersion remained. The chirp-mirror is a dielectric mirror coated with alternating dielectric films of aperiodically increasing depths designed as a variable delay-line device for spectral components of the incident fs-pulse (Fig. 5), i.e., A lower-frequency component is more delayed by reflection at a larger depth through more dielectric films while a higher-frequency component less delayed by a shallower depth reflection. This anomalous

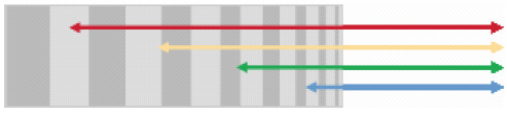

Fig. 5. Configuration of aperiodic dielectric layers of a chirp mirror as a variable delay-line for the spectral components of the incident fs-pulse [29].

chromatic dispersion induced by the chirp-mirror would cancel the normal dispersion to which the sub-10 fs pulse is subject when traveling through cuvette, dye-phantom, and ND filter. Nearly normal incidence of pulsed laser beam is required so that at each layer interface the reflectance $R = \left(\frac{n_{transmit} - n_{incident}}{n_{transmit} + n_{incident}}\right)^2$ and transmittance $T = \frac{4 n_t n_i}{(n_t + n_i)^2}$ are insensitive to polarization of incident fs-pulse beam, leading to consistent GDD compensation. The chirp-mirror has a number of advantages: space saving, convenience for alignment, and greatly diminished higher-order dispersion contributions owing to its very thin layers of dielectric materials (Fig. 6), which proves to work well as GDD compensation elements inside the Ti:Sapphire oscillator.

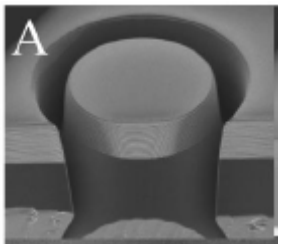

Fig. 6. An electron microscope image of a tiny dielectric mirror whose thin dielectric layers could be periodic or aperiodic (i.e., chirp-mirror) [30].

Additional GDD effect on both sub-10 fs and 140 fs pulse, which would have been caused by a telescope beam expander and an objective lens, is eliminated by the custom-designed dispersion-less beam expanding and focusing unit (see sub-section 2.2).

To achieve optimal GDD compensation by tentative installations of chirp-mirror pair, interferometric autocorrelation (IA) measurements are being made to estimate duration of the fs-pulse which is subject to both the positive GDD from the optical elements considered and the negative GDD provided by the chirp-mirror pair tentatively selected (recall Fig. 4B). The interferometric autocorrelator for IA trace measurements (FEMTOMETER^{TM}, FEMTOLASERS) works on the principles of a Michelson interferometer (Fig. 7) with specially coated and fabricated optical elements (e.g., beam-splitter/BS and BBO slice for SHG is less than 25μm thick) to minimize additional GDD effect involved in the pulse duration characterization. The incident laser pulse through

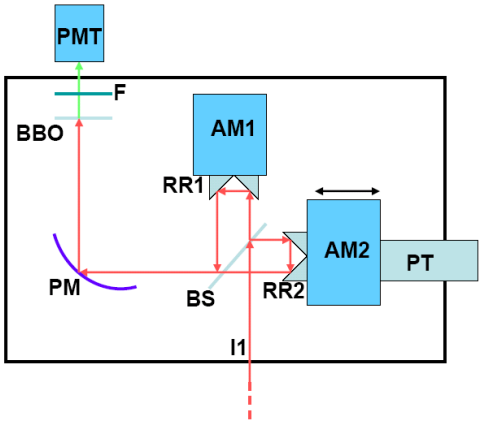

Fig. 7. Configuration of the interferometric autocorrelator [31].

the iris (I1) is split by the 50-to-50 beam-splitter (BS) to have the pulse and its copy respectively reflected by the stationary arm RR1&AM1 and by the scanning arm RR2&AM2 (driven by a piezoelectric-driver PT to vary relative time-delay τ_d in

between). As this time-delay scans, temporal overlap between the pulse and its copy shifts when they re-combine at the BS and co-propagate forward, which results in interference fringe signals in time domain to be focused by the parabolic mirror (PM) onto to the BBO slice for efficient SHG. The generated SHG signals after the BBO slice has the same fringe pattern as that in NIR regime before it. The fundamental beam involved in the SHG after the BBO is blocked by the filter (F) to have good signal-to-noise ratio (SNR) in detection of the SHG fringes by the PMT.

Initially, the intrinsic sub-10 fs mode-locked pulse from the un-tuned laser is characterized by its IA trace (Fig. 8a) measured with the interferometric autocorrelator.

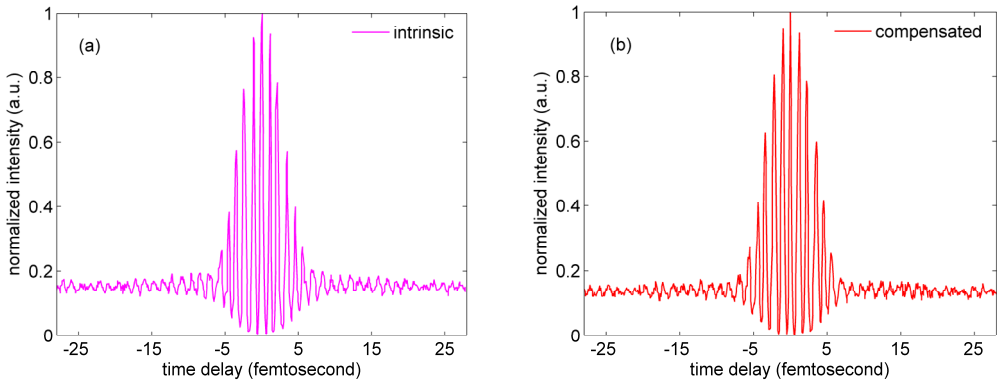

Fig. 8. Interferometric autocorrelation trace of (a) intrinsic sub-10 fs mode-locked pulse from the un-tuned laser agrees well with that of (b) GDD-compensated sub-10 fs TLP *in situ*.

Tentative trials of GDD compensation for delivering sub-10 fs TLP *in situ* are tested by

IA measurements and with a home-built 5.0-mm-path-length glass-chamber (two 150μm-thick microscopic cover-glass slices as windows) containing the dye-phantom, a 1.0mm-thick BK7 plate, and ND filter placed in the optical path (recall Fig. 4B). The optimal GDD compensation is finally achieved by one-pair of bounces off a rectangular chirp-mirror (GDD/bounce < −250 (±20) fs^2, GSM201, FEMTOLASERS) and a circular chirp-mirror (GDD/bounce < −45 (±10) fs^2, GSM001, FEMTOLASERS). The IA trace of the GDD-compensated sub-10 fs TLP *in situ* is shown in Fig.8b, in good agreement with that (Fig. 8a) of the intrinsic sub-10 fs mode-locked pulse for the satisfactory 8:1 peak-to-background ratio according to the expansion of the 2nd-order autocorrelation function [27]

$$
\begin{aligned}
I_{IA}(\tau_d) &= \int_{-\infty}^{\infty} \left| \{ E(t)\exp[i\omega t + i\Phi(t)] \right. \\
&\qquad \left. + E(t-\tau_d)\exp[i\omega(t-\tau_d) + i\Phi(t-\tau_d)] \}^2 \right|^2 dt \\
&= \int_{-\infty}^{\infty} \left| 2E^4 + 4E^2(t)E^2(t-\tau_d) \right. \\
&\qquad + 4E(t)E(t-\tau_d)\left[E^2(t) + E^2(t-\tau_d)\right]\cos[\omega\tau_d + \Phi(t) - \Phi(t-\tau_d)] \\
&\qquad \left. + 2E^2(t)E^2(t-\tau_d)\cos[2(\omega\tau_d + \Phi(t) - \Phi(t-\tau_d))] \right| dt \\
&= \begin{cases} 2^4 \int_{-\infty}^{\infty} E^4(t)dt \Big|_{\tau_d = 0} & (peak) \\ 2\int_{-\infty}^{\infty} E^4(t)dt \Big|_{\tau_d \to \infty} & (background) \end{cases}.
\end{aligned}
\tag{12}
$$

2.2 Combination of laser-beam expanding and focusing

In conventional TPEF spectroscopy [9], laser beam is expanded and focused into the sample with a telescope beam expander and an objective lens for TPEF measurements. This scheme for laser-beam expanding and focusing, which would have caused additional GDD effect on both sub-10 fs and 140 fs pulses, is replaced by a custom-

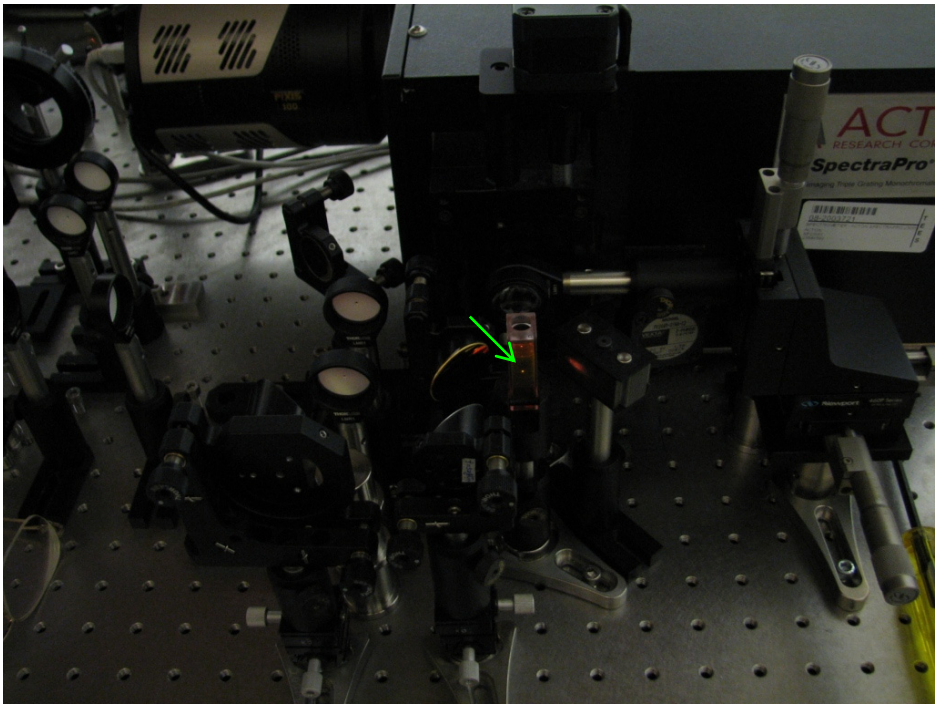

Fig. 9. Good optical sectioning is achieved by the custom-designed dispersion-less beam expanding and focusing with PM-combination. The axial IPSF *in situ* is much smaller than cuvette path-length.

designed unit of dispersion-less beam expanding and focusing (recall Fig. 4A) with three gold-coated 90˚ off-axis parabolic mirrors (with flat reflectivity greater than 95% in NIR ~ IR regime), i.e., PM1 (effective focal length/EFL, 20.32 mm, 50328AU, Newport), PM2 (EFL 50.8 mm, NT47-098, Edmund Optics), and PM3 (EFL 25.4 mm, NT47-096, Edmund Optics), each of which has two-dimensional tilt-adjustment and three-dimensional linear-translation for accurate alignment. This PM-combination is located at a distance from both laser exit apertures such that the beam size of the tunable 140 fs and un-tuned sub-10 fs pulses is ~ 4 mm and the effective numerical aperture (N.A.) for beam focusing ~ 0.2, corresponding to an estimated [32,33] axial intensity point spread function (IPSF) of ~ 400 μm by 1/e-width. This estimated IPSF *in situ*, is much smaller than cuvette path-length (see Fig. 9 for good optical sectioning achieved), making TPEF measurements insensitive to slight variations of laser beam size [9].

2.3 TPEF collection with a custom-designed compound-lens coupled to the spectrograph

To achieve efficient TPEF collection and good spectral resolution for accurate quantification of TPEF yield, a custom-designed [34,35] compound-lens (recall Fig. 4A) is assembled and well coupled to the spectrograph to form an integrated detection scheme. This compound-lens consists of two bi-convex lenses in contact (KBX043 with focal-length 19 mm, KBX046 with focal-length 25.4 mm, LKIT-1, Newport) optimally selected to achieve high N.A. and small projected image of the IPSF onto the entrance-slit of the spectrograph. The resultant compound-lens has an EFL of 13.75 mm, effective N.A. of ~ 0.3, and the IPSF projected image size of 147 μm, with the object-distance

(51.0 mm from the IPSF *in situ* to the effective front-principle-point) and image-distance (18.82 mm from the effective back-principle-point to the entrance-slit) designed for convenient phantom placement and compound-lens adjustment. A suitable lens-tube-holder mounted on a triple-stage allows the compound-lens tilt-adjustment and linear-translation. By setting the spectrograph in imaging mode and with a dye-phantom in place under laser excitation at ~ 20 mW power level, fine adjustment of the compound-lens is accomplished by monitoring the IPSF projected image on the CCD that is being relayed from the entrance-slit where the IPSF projected image by the compound-lens locates (recall Fig. 4A). Fig. 10A shows the IPSF projected image relayed onto the CCD

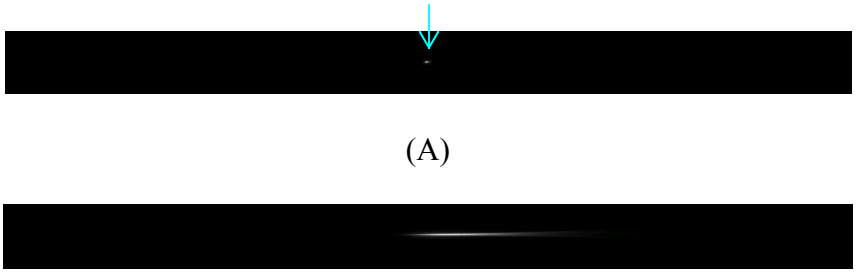

(A)

(B)

Fig. 10. (A) The IPSF projected image relayed onto the CCD camera; (B) the corresponding spectrum (in spectral mode).

camera aligned with the corresponding spectrum (Fig. 10B in spectral mode). The cuvette-holder is fixed on the optical table to ensure unchanged IPSF position with dye-phantom replacement.

The 300 grooves/mm (BLZ500 nm) grating is selected in the spectrograph (focal length 300 mm, Acton SpectrPro-2300i, Princeton Instruments) that is well focused onto

the CCD camera (1340×100, pixel size 20 μm, PIXIS100, Princeton Instruments). A bandpass filter (Schott BG39) is attached to the entrance-slit to block scattered laser light. With the entrance-slit width set at 200 μm (larger than the IPSF projected image size on the slit), spectral resolution of ~ 1.5 nm is achieved (calculated with the online "Grating Dispersion Calculator" at Princeton Instruments by using the IPSF projected image size 147 μm). This spectral resolution approaches the limit of this spectrograph if optical fiber coupling is used for fluorescence collection according to the user's manual.

2.4 Methodology

This experimental study on optimization of TPEF enhancement is made by direct comparison of TPEF yields for each single-dye phantom and a mixture of them excited by the un-tuned sub-10 fs TLP and by the 140 fs pulse tuned from 700 nm to 900 nm at 10 nm increment. To standardize this comparative study, quantities relevant to the measured TPEF enhancements are defined as follows. The normalized TPEF spectrum is defined as the measured TPEF spectrum normalized to the exposure-time (equivalently TPEF spectrum acquired per unit time). The normalized TPEF yield is defined as integrated value of the normalized TPEF spectral intensities (equivalently TPEF yield acquired per unit time). The measured TPEF enhancements are defined as ratio of the normalized TPEF yield by the sub-10 fs TLP to that by 140 fs pulse tuned to a specified wavelength. The TPE spectrum is defined as the normalized TPEF yields versus 140 fs pulse tuned wavelengths, whose profile is normalized to its peak.

In order to get insight into the physics behind the TPEF enhancements observed, a semi-quantitative discussion is made by comparison between the measured TPEF enhancements and the calculated ones and by illustration of relative spectral positions of the dye-molecule 1^{st}-excited singlet states versus laser frequencies together with a generalized Jablonski diagram. Special attention is given to the differentiated TPEF enhancements among the three dye-phantoms of distinct TPEF characteristics that are representative of fluorescent probes with similar properties. The conclusions made from these case studies are generalized to evaluation on two-photon excitation capability of the broadband fs-pulse excitation in terms of the fs-pulse SH power spectrum. The observations and discussions made on single-dye TPEF enhancements pave the way to the phantom study on multicolor TPEF enhancements with a mixture of the three dye-phantoms. This followed-up study is to explore an efficient excitation scheme with the un-tuned sub-10 fs TLP instead of compromised excitation schemes with tunable narrowband fs-pulses. Significance of this phantom study is highlighted by numerical simulations of OPA and solvent effects on multicolor TPEF profiles, which shows great promise of the broadband fs-pulse excitation for optimization of multicolor TPEF enhancement with environmental influences taken into account.

Prior to this comparative study, debugging of the integrated experimental setup with the custom-designed optical components are iteratively carried out through tentative TPEF measurements by stepwise increasing excitation powers at the preparatory steps of the square-law dependence study. In the meantime systematic improvement is made accordingly and TPEF characteristics of the three dye-phantoms

and hands-on experiences with this home-built system are gained, which are valuable to designing and revising the experimental protocol for the actual TPEF measurements.

The three single dye-phantoms are prepared all at 100 μM concentration [9] with Indo-1 (SKU#1-1202, Invitrogen) and FITC (F3651, Sigma-Aldrich) dissolved in deionized water, and TRITC (87918, Sigma-Aldrich) dissolved in methanol. The mixture is prepared at the volume-ratio of 27:17:1 with the three ready single dye-phantoms according to their relative brightness recognized in the single-dye TPEF measurements.

CHAPTER III

RESULTS AND DISCUSSION

3.1 The square-law dependence study

The square-law dependence of TPEF yield $\langle F(t) \rangle$ on laser excitation power $\langle P_{laser}(t) \rangle$ is formulated by Eq. (1) [4,9] which includes all the parameters related to experimental conditions and TPEF characteristics of the dye-molecule. As preparatory steps for this comparative study on TPEF enhancement, the square-law dependence study is particularly important for two reasons. First, the integrated experimental setup for all TPEF measurements includes two excitation schemes and custom-designed detection, which requires systematic debugging. Through tentative TPEF measurements in the square-law dependence study, overall performance of the experimental system could be evaluated and improved by re-alignment. Second, the three dye-phantoms of choice have their TPEF characteristics representative of fluorescent probes with similar properties, such as their TPE spectrum peak positions in relation to the sub-10 fs TLP SH power spectrum, TPEF emission peak positions, and relative brightness, which could be familiarized through these preparatory steps and suggest the protocol for the actual TPEF measurements to be made. Ultimately, to affirm non-resonant TPEF and avoid fluorescence saturation as well as higher-order nonlinearities [36], a suitable excitation power level is to be determined for both excitation schemes and with all three dye-phantoms, making this comparative study of TPEF enhancement on an equal basis. This square-law dependence study is first conducted with the 140 fs pulse tuned to 730 nm

(for Indo-1), 800 nm (for FITC), and 840 nm (for TRITC) (corresponding to the largest TPA cross sections of the three dyes, see Eq. (13)) where subtle deviations from the square-law suggest onsets of fluorescence saturation or higher-order nonlinearities

$$\begin{cases} \sigma^{TPA}_{S_0 \to S_f}\left(\lambda_{laser} = 730nm\right)\Big|^{Indo}_{MAX} \\ \sigma^{TPA}_{S_0 \to S_f}\left(\lambda_{laser} = 800nm\right)\Big|^{FITC}_{MAX} \\ \sigma^{TPA}_{S_0 \to S_f}\left(\lambda_{laser} = 840nm\right)\Big|^{TRITC}_{MAX} \end{cases} \tag{13}$$

with respect to the entire tuning range of 140 fs pulse excitation. Fluorescence spectra of the three dye-phantoms excited respectively at those tuned wavelengths are measured by increasing excitation powers from 10 mW to 150 mW at 5 mW increment measured with a thermopile sensor of broadband flat spectral response (spectral window 190 nm ~ 11000 nm, 818P-001-12, Newport) and a power meter (Model 1835-C single-channel optical meter, Newport). The fluorescence yields obtained by integrating fluorescence spectral intensities are plotted versus the excitation powers in logarithmic scale (Fig. 11) with the square-law slope of 2 as reference line. The fluorescence yields versus excitation powers likewise measured with the un-tuned sub-10 fs TLP excitation are shown in Fig. 12. Deviations from the square-law slope of 2 occur for all three dye-phantoms and both fs-pulse excitations at powers above 40 mW. Conservatively, excitation power of 20 mW is used for all the actual TPEF measurements.

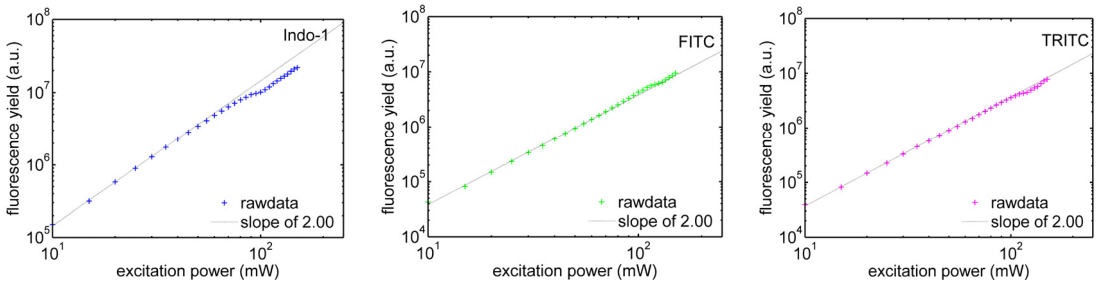

Fig. 11. Logarithmic plots of fluorescence yields versus excitation powers (10 mW ~ 150 mW at 5 mW increment) with 140 fs pulse tuned to 730 nm, 800 nm, and 840 nm respectively for Indo-1, FITC, and TRITC. Dash-lines with slope 2 are shown for reference.

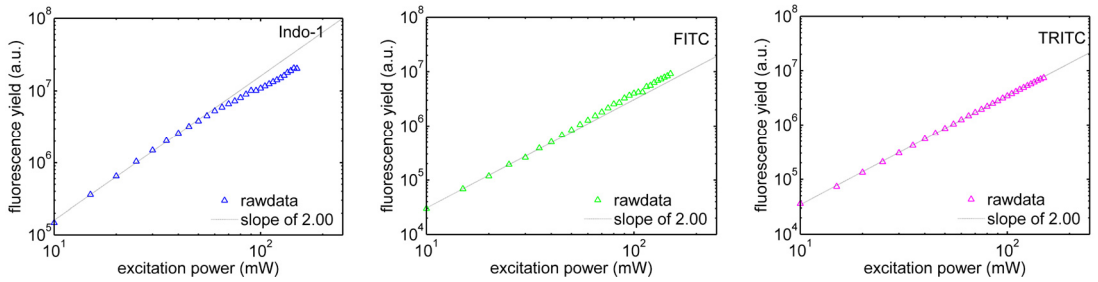

Fig. 12. Logarithmic plots of fluorescence yields versus excitation power (10 mW ~ 150 mW at 5 mW increment) with the sub-10 fs TLP for Indo-1, FITC, and TRITC. Dash-lines with slope 2 are shown for reference.

3.2 TPEF enhancements by direct comparison

TPEF spectra excited by the un-tuned sub-10 fs TLP and 140 fs pulse tuned from 700 nm to 900 nm at 10 nm increment are measured with excitation power set at 20 mW. In the three-dimensional framework of Fig. 13, the normalized TPEF spectra (X- and Z-axis) of each dye-phantom are shown with reference to laser excitations of the un-tuned sub-10 fs TLP at 792 nm and the 140 fs pulse tuned from 700 nm to 900 nm at 10 nm increment (Y-axis).

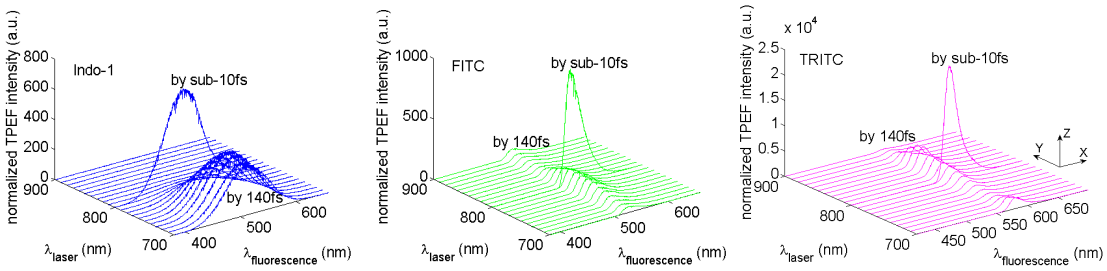

Fig. 13. Normalized TPEF spectra (X- and Z-axis) of Indo-1 (peaked at 498 nm), FITC (peaked at 523 nm), and TRITC (peaked at 578 nm) shown in three-dimensional framework with reference to laser excitations of sub-10 fs pulse at 792 nm and 140 fs pulse tuned from 700 nm to 900 nm (Y-axis).

The normalized TPEF spectral peak of each dye-phantom does not shift with the excitation wavelength tuning whereas overall TPEF enhancements by the un-tuned sub-10 fs TLP for the three dye-phantoms are readily observed at each tuned wavelength of

the 140 fs pulse, showing noticeable advantage of the un-tuned broadband fs-pulse over the tunable narrowband fs-pulse excitation. The TPEF enhancements by direct comparison are quantified at each tuned wavelength of 140 fs pulse (bar-graphs in Fig. 14), from which special attention is given to the enhancements of 1.6 (for Indo-1 at 730 nm tuned wavelength), 6.7 (for FITC at 800 nm tuned wavelength), and 5.2 (for TRITC at 840 nm tuned wavelength). Those tuned wavelengths of 140 fs pulse excitations are

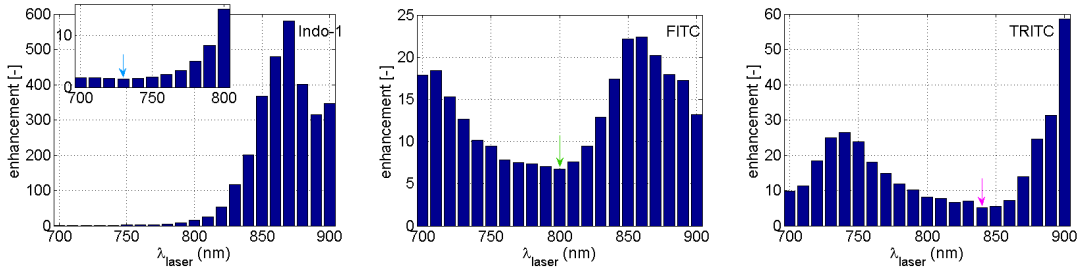

Fig. 14. TPEF enhancements by direct comparison between sub-10 fs TLP and 140 fs pulse tuned from 700 nm to 900 nm at 10 nm increment, esp. those at tuned wavelengths of 730 nm (for Indo-1), 800 nm (for FITC), and 840 nm (for TRITC).

respectively optimal for Indo-1, FITC, and TRITC to have their maximum TPEF yields (Fig. 13), corresponding to their TPE spectrum peak positions (Figs. 15-17) where the three dye-molecules exhibit the largest TPA cross section (Eq. (1) and Eq. (13)). This way of determining the optimal wavelength for a specific dye-molecule by the TPE spectrum peak position could in principle be applied to optimization of TPEF

enhancement with narrowband fs-pulse tuning. In practice, the optimal wavelength is usually determined through tentative trials of imaging with TPM. Then, a question arises about tradeoff between tunability of narrowband fs-pulse and un-tuned broadband fs-pulse excitations for TPEF enhancement. These observations (Figs. 13-14) suggest that de-tuning of the sub-10 fs pulse (centered at 792 nm) relative to the TPE spectrum peak positions (Figs. 15-18) of the three dye-phantoms does not necessarily diminish capability of the sub-10 fs TLP for TPEF enhancement owing to its high peak power and broad bandwidth. The differentiated TPEF enhancements among the three dye-phantoms at those tuned wavelengths of the 140 fs pulse excitation give further implications. First, the effective TPEF enhancement should be related to both the fs-pulse SH power spectrum and the TPEF characteristics (i.e., TPE versus OPA spectrum in Figs. 15-17) of a specific dye-molecule, which typifies the semi-classical style [4] in the theoretical discussion (sub-section 3.3), i.e., to treat the fs-pulse excitation classically (fs-pulse SH power spectrum) and the dye-molecule quantum-mechanically (TPE versus OPA spectrum). Secondly, results of the case studies by the two excitations and the three dye-phantoms of distinct TPEF characteristics could be extended to fluorescent probes of similar properties and give hints at better utilization of broadband fs-pulse excitations for optimization of multicolor TPEF enhancement (see sub-section 3.4).

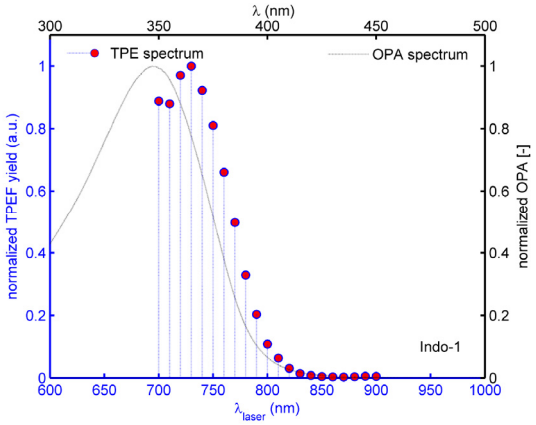

Fig. 15. TPE spectrum of Indo-1 peaks at 730 nm tuned wavelength of 140 fs pulse in reference to the corresponding OPA spectrum.

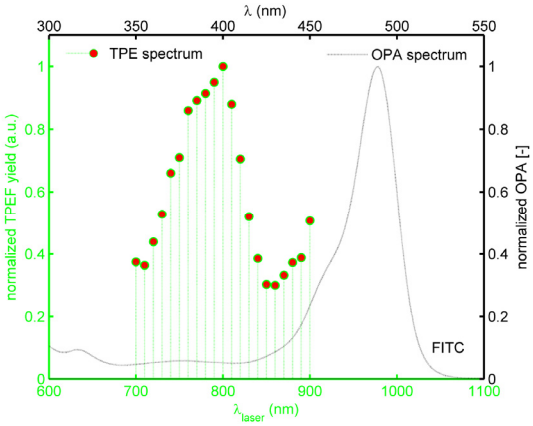

Fig. 16. TPE spectrum of FITC peaks at 800 nm tuned wavelength of 140 fs pulse in reference to the corresponding OPA spectrum.

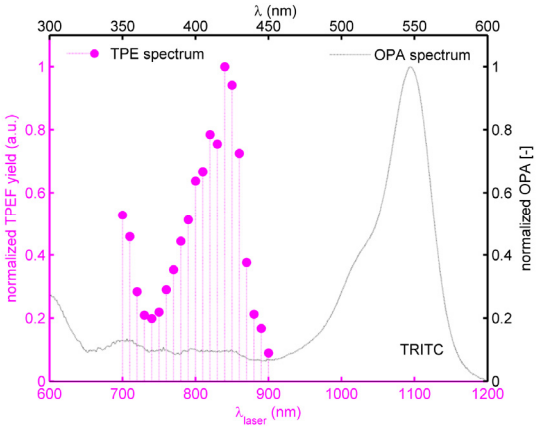

Fig. 17. TPE spectrum of TRITC peaks at 840 nm tuned wavelength of 140 fs pulse in reference to the corresponding OPA spectrum.

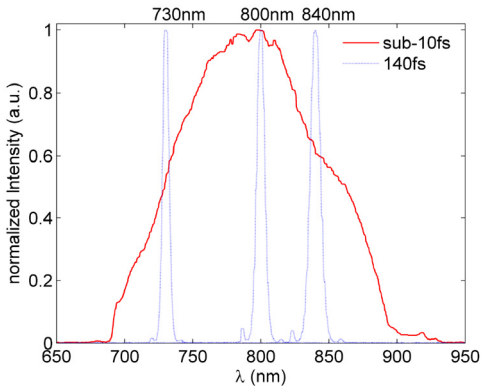

Fig. 18. Laser spectra of sub-10 fs pulse at 792 nm and 140 fs pulse tuned to 730 nm, 800 nm, and 840 nm.

3.3 TPEF enhancements by calculation

To evaluate TPEF enhancements by calculation and to make a theoretical discussion on the physics behind TPEF enhancements, TPE spectra of the three dye-phantoms obtained from the normalized TPEF yields with 140 fs pulse excitation are shown in Figs. 15-17 together with the corresponding OPA spectra (measured by a PerkinElmer Lambda 45 UV/Vis spectrometer) for reference to their relative spectral positions [3]. Laser spectra of sub-10 fs pulse and the 140 fs pulse tuned to 730 nm, 800 nm, and 840 nm are shown in Fig. 18 for further reference. It could be recognized from the TPE versus OPA spectrum [37] that two-photon absorption by narrowband fs-pulse tuning variously excites dye-molecule to TPA-associated final states energetically degenerate with (e.g., Indo-1) and (e.g., FITC), or higher (e.g., TRITC) than OPA-associated 1st-excited singlet state [3]. Expectedly, such various excitations could be simultaneously achieved *via* both degenerate ($\nu_1 = \nu_2$) and non-degenerate ($\nu_1 \neq \nu_2$) TPA with the spectral FWTM (~ 190 nm) of un-tuned sub-10 fs pulse closest to the tuning range of 140 fs pulse. In this manner, the broadband fs-pulse excitation allows for more accessibility to TPA-associated final states and diversely promotes population of thus excited dye-molecules, leading to differentiated TPEF enhancements. It is readily seen from Eq. (1) that measured TPEF enhancement (i.e., ratio of normalized TPEF yields) is proportional to ratio of two-photon transition probabilities [4] $\frac{\Gamma_{TPA}|_{10\,fs}}{\Gamma_{TPA}|_{140\,fs}^{\lambda_{laser}}}$ of each dye-molecule by sub-10 fs TLP versus 140 fs pulse tuned to a wavelength, i.e.,

$$\text{TPEF enhancement} = \left.\frac{\langle F(t)\rangle_{10\,fs}}{\langle F(t)\rangle_{140\,fs}^{\lambda_{laser}}}\right|_{measured} \propto \left.\frac{\Gamma_{TPA}|_{10\,fs}}{\Gamma_{TPA}|_{140\,fs}^{\lambda_{laser}}}\right|_{calculated}. \qquad (14)$$

The relevant two-photon transition probability Γ_{TPA} for each dye-molecule can be calculated according to the phenomenologically introduced formula Eq. (3) [23] by using interpolated data of the TPE spectrum $\gamma(\omega)$ of the dye-phantom (refer to Figs. 15-17) and fs-pulse SH power spectrum $\left|\int_0^\infty A\left(\frac{\omega}{2}+\Omega\right)A\left(\frac{\omega}{2}-\Omega\right)d\Omega\right|^2$ converted from the measured laser spectrum with no phase terms introduced, assuming transform-limited pulses. The fs-pulse SH power spectrum in Eq. (3) resulted from Fourier transform of the electric field of the excitation pulse [23] reflects the fact that both degenerate and non-degenerate TPA are allowed with the frequencies of all possibly paired photons lying within the TLP spectrum. The calculated TPEF enhancements at those tuned wavelengths of the 140 fs pulse excitation are summarized in Table 1, which are in proportional agreement with the measured ones, i.e., Indo-1 of the lowest TPEF

Table 1. Measured and calculated TPEF enhancements

central wavelength of tunable 140 *fs* pulse	**730 nm**	**800 nm**	**840 nm**
ratios of integrated SH power spectrum (sub-10 *fs* pulse : tunable 140 *fs* pulse)	13.5	12.1	11.3
Organic Dye Phantoms	**Indo-1**	**FITC**	**TRITC**
measured TPEF enhancements	1.6	6.7	5.2
calculated TPEF enhancements	3.4	13.3	8.0

enhancement, FITC of the highest, and TRITC of the secondary. The difference between measured and calculated enhancements could be ascribed to residual phase distortions in

the broadband and narrowband fs-pulses because of imperfect GDD compensation, slight mismatch of pulse-repetition-rates between the two fs-pulse excitations, and difference in fluorescence collection efficiencies. The differentiated TPEF enhancements among the three dye-phantoms excited at those tuned wavelengths of the 140 fs pulse excitation originates in the overlap between the dye-molecule TPE spectrum and the fs-pulse SH power spectrum that is formulated as the overlap integral in Eq. (3).

To generalize the differentiated TPEF enhancements by assuming invariant frequency response of dye-molecule (i.e., TPE spectrum be independent of laser frequency), calculation of two-photon transition probability by Eq. (3) is simplified to integral of the fs-pulse SH power spectrum, which is indicative of two-photon excitation capability of the transform-limited fs-pulse. For measured laser spectra (Fig. 18), ratio of the integrated SH power spectrum of sub-10 fs pulse to that of 140 fs pulse is upper limited to 14, from which the ratio decreases due to non-identical pulse shapes [15] of sub-10 fs and 140 fs pulse whose spectral area increases as tuned to longer wavelengths.

The proportional agreement between the measured and calculated TPEF enhancements suggests that optimization of TPEF enhancement does not depend solely on narrowband fs-pulse tuning but ultimately on the overlap of the fs-pulse SH power spectrum with the dye-molecule TPE spectrum. The assumed transform-limited fs-pulse best demonstrates the distinct advantage of the un-tuned fs-pulse with broad SH power spectrum over the tunable narrowband fs-pulse for TPEF enhancement. Fig. 19 (relative

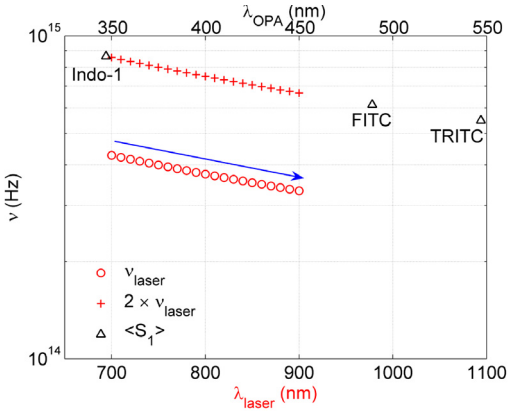

Fig. 19. Semi-logarithmic plots of relative spectral positions (in Hz and nm) of 1st-excited singlet state $<S_1>$ of the dye-molecule recognized from the OPA spectra in Figs. 15-17 in reference to 140 fs pulse SH frequencies ($2\times\nu_{laser}$) and tuning range that well approximates spectral FWTM of the sub-10 fs TLP.

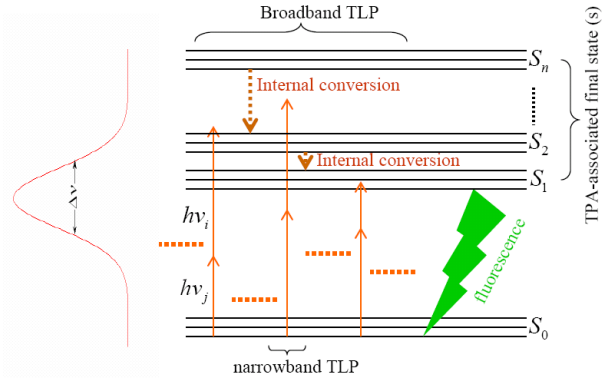

Fig. 20. The generalized Jablonski diagram illustrates physics behind the differentiated TPEF enhancements among the three dye-phantoms.

spectral positions vertically represented in frequency domain with reference to Figs. 15-18) and Fig. 20 (generalized Jablonski diagram) comprehensively illustrate the physics behind the differentiated TPEF enhancements among the three dye-phantoms, i.e., With the broadband sub-10 fs TLP readily involved in both degenerate and non-degenerate TPA, this un-tuned ultrashort fs-pulse excitation simultaneously allows for more accessibility to TPA-associated final states of the dye-molecule and diversely promotes population of thus excited dye-molecules among the three dye-phantoms with their distinct TPE spectra. This advantage with the broadband fs-pulse excitation may be mitigated when the dye-molecule TPE spectrum peak position would fall off the fs-pulse SH power spectrum, leading to a diminished overlap (e.g., fluorescent protein variants Venus and DsRed [38]). Nonetheless, the measured and calculated TPEF enhancements suggest a competitive advantage in optimization of TPEF enhancement by coherent quantum control of broadband fs-pulse for selective excitation [39-41] over narrowband fs-pulse wavelength tuning. This method of dynamically responding to multiple-dye labeled bio-samples via feedback-loop automation achieves spectral tailoring of broadband fs-pulse with high efficiency, facilitating selective excitation for various imaging tasks.

3.4 Multicolor TPEF enhancements and solvent effects

The differentiated TPEF enhancements observed among the single dye-phantoms give rise to further consideration about optimization of multicolor TPEF enhancement. A phantom study with a mixture of the three single dye-phantoms is made to explore multicolor TPEF enhancements. To facilitate observation of multicolor TPEF spectrum, this mixture is prepared by mixing the three single dye-phantoms at the volume ratio of 27:17:1 according to their brightness recognized from the TPEF measurements described in sub-section 3.2 (recall Fig. 13). To clarify some issues related to environmental influences on multicolor TPEF profiles, numerical simulations on OPA and solvent effects are carried out with measured data from diluted single dye-phantoms.

Compared to single-color imaging by TPM and with single-dye labeled samples, optimization of multicolor TPEF enhancement for TPM with multiple-dye labeled samples is more difficult to achieve because of entangled influences on multicolor TPEF spectrum, such as spectral resolution related to detection schemes, temporal resolution related to simultaneous excitation of multiple fluorescent probes and image acquisition rate, and discernability of multicolor TPEF profile and detectability of multiple fluorescent probes, to name a few. One approach to help produce spectral cross-talk free images is to sequentially capture single-color images of a multiple-dye labeled bio-sample by rapidly tuning narrowband fs-pulse to the wavelengths optimal for those fluorescent labels [42]. However, this approach demands well-separated excitation and emission spectra and may impose limitations to *in vivo* time-course studies where good temporal resolution is desired. Another approach is to split a broadband fs-pulse train,

shape each to selectively excite a different fluorescent probe and recombine with pulses interlaced for excitation "switching" at twice the laser repetition rate [43]. This approach does not compromise image acquisition rate, but extension to more than two fluorescent probes may be complicated by TPEF lifetimes and laser pulse-repetition-rate, and hence, the resultant "switching" rate. Alternatively, the sub-10 fs pulse with broad SH power spectrum may well facilitate simultaneous excitation of multiple fluorescent probes to have enhanced multicolor TPEF images, and together with multi-channel spectral detection schemes, to acquire respective "TPEF emission fingerprints"[2] efficiently for un-mixing and image segmentation [44-47].

Normalized multicolor TPEF spectra (Fig. 21) are acquired from this mixture excited by the un-tuned sub-10 fs TLP and by the 140 fs pulse tuned to 730 nm, 800 nm, and 840 nm (both at 20 mW excitation power level). Consistent with the TPEF enhancements in single dye-phantoms (recall Figs. 13-14), the multicolor TPEF signals with the mixture are overall stronger when excited by the un-tuned sub-10 fs TLP than by the tunable 140 fs pulse, regardless of its central wavelength. For each constituent dye in the mixture, variation of TPEF peak intensity in reference to 140 fs pulse wavelength tuning is also observed, which shows a compromised excitation scheme for multiple fluorescent probes inherently with narrowband fs-pulse tuning, i.e., Optimal excitation of one dye by narrowband fs-pulse tuning could be achieved at the expense of deficient excitation of others. Consequently, the discernability of measured multicolor TPEF spectrum is somewhat reduced (e.g., FITC- and TRITC-related peaks in Fig. 21a),

[2] i.e., single-color TPEF spectral peak positions representative of constituent fluorescent labels.

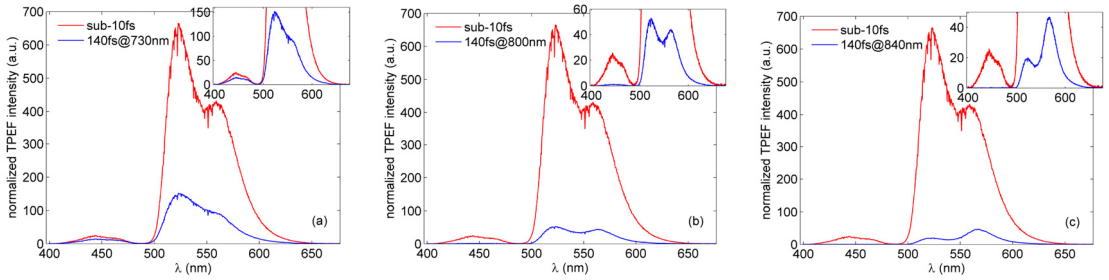

Fig. 21. Normalized multicolor TPEF spectrum of the mixture with the single dye-phantoms of Indo-1, FITC, and TRITC mixed at the volume-ratio 27:17:1, excited by sub-10 fs TLP and by 140 fs pulse tuned to (a) 730 nm, (b) 800 nm, and (c) 840 nm. Recall Fig. 13 for single-color TPEF spectral peak positions of the constituent dye-phantoms.

or, the measured multicolor TPEF spectrum gives misleading information about relative concentrations among the constituent dye-molecules (e.g., the highest TRITC-related peak in Fig. 21c uncorrelated to its lowest concentration in the mixture). This observation is particularly acute for Indo-1 whose TPEF signal could hardly be evident when the mixture is excited by the 140 fs pulse tuned to 800 nm optimal for FITC (Fig. 21b) and to 840 nm for TRITC (Fig. 21c).

It should be noted that the sub-10 fs TLP excitation at 792 nm is detuned off the TPE spectrum peak positions of 730 nm (for Indo-1) and 840 nm (for TRITC). Nevertheless, the un-tuned sub-10 fs TLP with its broad SH power spectrum appreciably overlapping the dye-molecular TPE spectra lessens this detuning effect, showing its

promise as an efficient excitation scheme capable of simultaneous excitation of the constituent dyes. Good detectability of multiple fluorescent probes with the broadband fs-pulse excitation could not be well recognized without considering extensive overlap of its broad SH power spectrum with the dye-molecule TPE spectra of interest. In analogy to incoherent broadband excitation for one-photon excited fluorescence (OPEF) [3], simultaneous excitation with broadband fs-pulses extensively promotes populations of thus excited constituent dye-molecules, beyond capability of compromised excitations by narrowband fs-pulse tuning. It is also observed that the multicolor TPEF spectrum from the mixture does not resemble simply a linear summation of TPEF spectra from the single dye-phantoms. A number of factors could contribute to this observation such as overlap of TPEF emission and OPA spectra [48] and environmental influences [49], on which numerical simulations with measured data are carried out for clarification.

To explore the way of making numerical studies on the OPA and solvent effects on multicolor TPEF spectrum, the three single-color TPEF spectra (Indo-1, FITC, and TRITC) by the sub-10 fs TLP (sub-section 3.2) are multiplied by their respective volume-ratio in the mixture (i.e., “numerically diluted”) because TPEF yield is proportional to dye-phantom concentration (Eq. (1)). These intensity-reduced TPEF spectra from “numerical dilution”, corresponding to the ones from physically-diluted dye-phantom doses in the mixture, are plotted together with their linear summation. The resultant “multicolor TPEF spectrum” (dash-black line in Fig. 22a) exhibits marked differences from the measured one (solid-line in Fig. 22c). Spectral overlaps(s) of TPEF emission (blue-, green-, and red-line in Fig. 22a) and OPA (Fig. 22b) among the three

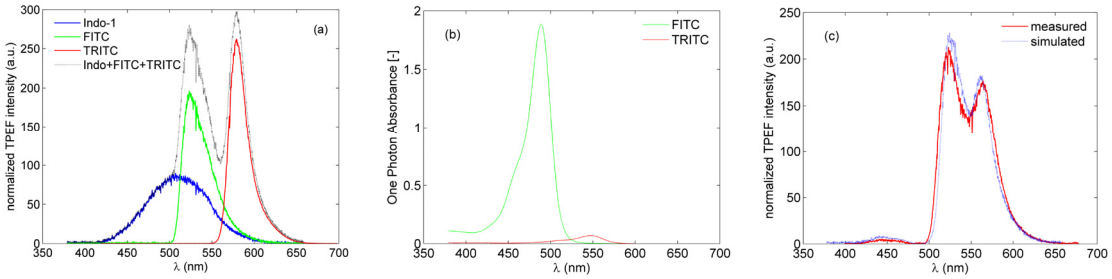

Fig. 22. (a) Individual and linear summation (dash-black) of Indo-1 (blue), FITC (green), and TRITC (red) TPEF spectra, (b) OPA spectra of FITC (green) and TRITC (red), and (c) measured (red) and simulated (blue) TPEF spectra of the mixture clarify OPA contributions from FITC- and TRITC-molecules and solvent effect on TRITC.

constituent dyes suggest OPA effects, i.e., Indo-1 TPEF emission is subject to OPA by FITC and TRITC molecules while FITC TPEF emission to OPA by TRITC molecule. The corresponding OPA spectra (Fig. 22b) are measured with the FITC- and TRITC-phantom dose in the mixture diluted respectively by water plus methanol and by water, of volumes equivalent to those of the other two constituent dye-phantom doses in the mixture. Based on Beer's law, the OPA effect on the linear summation of single-dye TPEF spectra are simulated (blue-dash line in Fig. 22c) together with the measured (red-solid line in Fig. 22c) multicolor TPEF spectrum from the mixture. Good agreement between measurement and simulation confirms significant OPA contribution from FITC and TRITC molecules. In addition, a solvent effect is found to contribute to the blue-

shift and intensity drop at TRITC-related peak in the multicolor TPEF spectrum, to which similar observations were reported recently [50]. This solvent effect [51] resulted from dilution is included in the OPA simulation by using the TPEF spectrum from TRITC-phantom dose diluted by water of volume equivalent to that of the other two constituent dye-phantom doses in the mixture. This solvent effect due to water dilution happens only to TRITC-phantom dose in the mixture, which is elucidated as follows. Fig. 23 shows that the TPEF spectral peak of TRITC phantom (water as solvent) blue shifts by 10 nm and drop to ~ 650 (a.u.) from that of TRITC phantom (MeOH as solvent) (both at 100 μM concentration), which agrees with recent observations of this

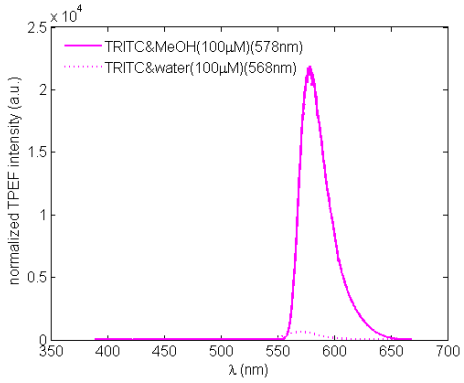

Fig. 23. TPEF spectral peak of TRITC & water phantom blue shifts by 10 nm and drops to ~ 650 (a.u.) from that of TRITC & MeOH phantom.

solvent effect [50,51]. In the above-mentioned OPA simulation, the TPEF spectrum of TRITC-phantom dose diluted by water is used, whose peak blue shifts by 13 nm and drop to ~ 115 (a.u.) (Fig. 24), which can be interpreted as combination of this solvent

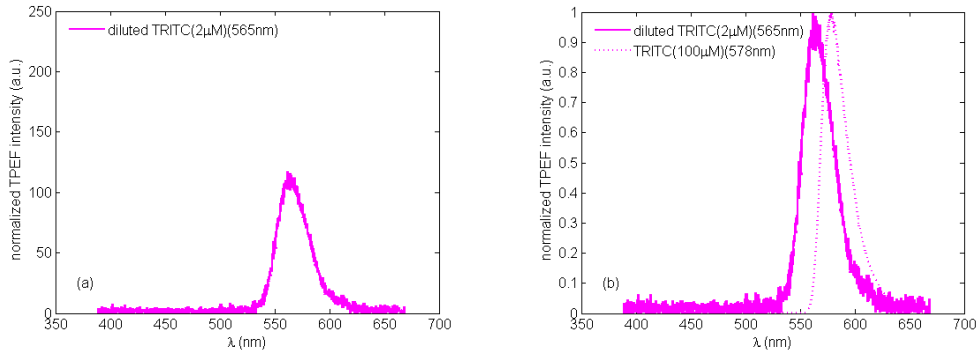

Fig. 24. The TPEF spectral peak of TRITC-phantom dose diluted by water of volume equivalent to that of the other two constituent dye-phantom doses in the mixture (a) drops to ~ 115 (a.u.) and (b) blue shifts by 13 nm.

effect and dilution, of which the latter is responsible for additional blue-shift and intensity drop from reduction of self-quenching (S-Q) effect at low concentration (~ 2 μM). S-Q effect by definition means that fluorescence emission from the dye-molecules is one-photon absorbed by themselves whose OPA spectrum overlaps with its fluorescence spectrum to some extent [51]. Direct consequence of S-Q effect is distortion of fluorescence spectrum in terms of spectral peak shift and drop, which is dependent on dye-phantom concentration. While S-Q effect on Indo-1 and FITC is unnoticeable because of negligible overlap between their OPA and TPEF spectra,

considerable overlap exits between OPA and TPEF spectra of TRITC-phantom (Fig. 25), which accounts for reduced S-Q effect as a minor part (i.e., additional 3 nm blue-shift and 535 (a.u.) drop in fluorescence intensity) in the resultant TPEF spectral peak blue-shift and intensity reduction (Fig. 24) with TRITC-phantom dose diluted by water.

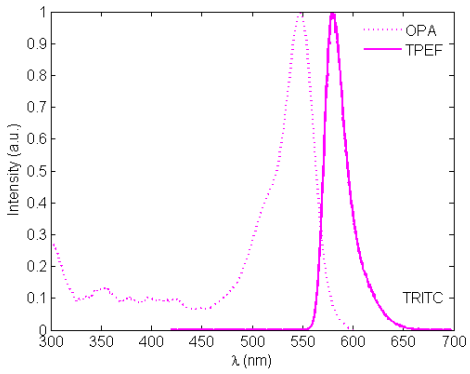

Fig. 25. Considerable overlap between OPA and TPEF spectra of TRITC-phantom accounts for reduced S-Q effect by dilution which plays a minor part in the TPEF peak blue-shift and drop shown in Fig. 24.

In principle, such S-Q effect induced fluorescence spectrum distortion with TPEF is much less prominent than that with OPEF [9]. In contrast, the OPEF spectra of TRITC-phantom (MeOH as solvent and initially at 100 μM concentration, measured with PC1 photon counting steady-state spectrofluorimeter, ISS) stepwise diluted by water are shown in Fig. 26, where distorted OPEF spectrum of the TRITC-phantom

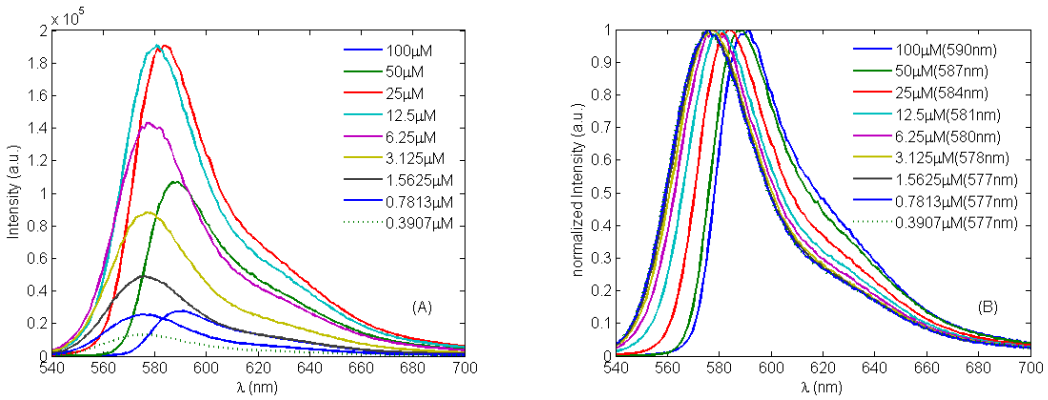

Fig. 26. Gradually reduced S-Q effect by stepwise dilution of TRITC-phantom shows (A) spectral peak variation and (B) blue-shift, resulting in the stabilized OPEF spectrum at low concentration (~ 2 μM).

at high concentration gradually approximates the stabilized one at low concentration (~ 2μM), indicating gradual reduction of S-Q effect by stepwise dilution. The difference in the resultant TPEF and OPEF spectra (Fig. 27) *both* with the TRITC-phantom dose at low concentration (~2 μM) by water dilution shows less distortion by reduced S-Q effect with TPEF than that with OPEF, though they are related to the *same* solvent effect on TRITC. This phenomenon can be ascribed to different excitation manners, i.e., fs-pulse train excitation of MHz pulse-repetition-rate with TPEF versus continuous-wave excitation with OPEF, of which the latter with much greater fluorescence yield thus excited and due to larger OPA cross section causes excessive intensity build-up on red-side of fluorescence spectrum under no influence of S-Q effect. On the other hand, blue-

side of fluorescence spectrum is subject to S-Q effect, leading to intensity reduction therein. Consequently, resultant fluorescence spectral peak red shifts with the TRITC-phantom at high concentration and blue shifts as reduction of S-Q effect is going on by water dilution.

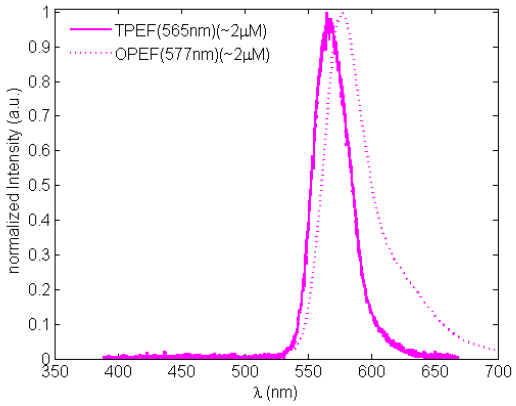

Fig. 27. The difference in the resultant TPEF and OPEF spectra both with the TRITC-phantom dose at low concentration shows less distortion by reduced S-Q effect with TPEF than that with OPEF, though related to the same solvent effect on TRITC.

All the above-made observations illustrate some issues relevant to multicolor molecular imaging with TPM, in particular, perturbed TPEF profiles from OPA and environmental effects. In practice, frequency dependence of optical scattering in tissues [52] could further modulate TPEF profiles, though this effect is not studied here. Implied in these observations is the importance of dispersion management for broadband fs-pulse

excitations to optimize single- or multicolor TPEF enhancements. For TPM with sub-10 fs pulse excitation scheme, dispersion management is non-trivial but has been demonstrated [21,53].

CHAPTER IV

CONCLUSIONS

This research project comprehensively explores optimization of TPEF enhancement in aspects of (1) inverse proportionality of TPEF yield to fs-pulse duration (in time domain), (2) tradeoff between tunability of narrowband fs-pulse and un-tuned broadband fs-pulse by case studies with three carefully selected dye-phantoms representative of fluorescent probes with similar TPEF characteristics (in frequency domain), (3) a semi-classical analysis on the differentiated TPEF enhancements (measured and calculated) among the three dye-phantoms, (4) demonstration of multicolor TPEF enhancement by effectively simultaneous excitation of constituent dyes in the mixture with the un-tuned broadband sub-10 fs TLP, and (5) phantom and numerical studies of environmental influences (OPA and solvent effects) on constituent dyes in the mixture.

The time-domain study points out that the inverse proportionality of TPEF yield versus laser pulse duration is best observed by transform-limited pulse of durations greater than 40 fs, where frequency dependence of TPA cross section is negligible. This inverse proportionality in principle characterizes optimization of TPEF enhancement in narrowband fs-pulse regime and can be readily applied to practical imaging because of negligible GDD effect herein. As the fs-pulse duration declines into the broadband regime (i.e., < 40 fs), GDD effect on the incident broadband fs-pulse becomes prominent and frequency dependence of TPA cross section (or, dye-molecule frequency variant response) is no longer negligible, which results in various deviations from the inverse

proportionality. Trends of deviation from the inverse proportionality are characteristic of the overlap between broadband fs-pulse SH power spectrum and dye-molecule TPE spectrum, which can be better understood through frequency-domain study.

The follow-up comparative study in frequency-domain is made by un-tuned sub-10 fs TLP versus tunable 140 fs pulse excitation with custom-designed GDD compensation and dispersion-less laser-beam expanding and focusing for delivery of nearly transform-limited fs-pulse *in situ*. Optical elements involved in TPEF measurements are mainly responsible for overall GDD effect due to their large thickness. Comparatively, the accumulative GDD effect by dye-phantom, cuvette, and ND filter is minor, for which optimal GDD compensation is accomplished by merely one-pair of bounces on chirp-mirrors with the sub-10 fs pulse excitation and for which GDD compensation with narrowband fs-pulse excitation can be neglected. In practical imaging, GDD effect from a thick bio-sample could be negligible for narrowband fs-pulse excitation but may require dispersion management for broadband fs-pulse excitation. In order to make best use of the un-tuned sub-10 fs pulse excitation, special attention should be given to GDD compensation design and spectral window of optical elements in the microscope system to achieve optimization of TPEF enhancement *in situ*. In general, GDD compensation with chirp mirrors cannot be perfect due to a number of reasons. The broadband fs-pulse may not match the bandwidth limit of chirp-mirrors perfectly. Radial dependence of refractive index in the microscope system may cause in-homogenous GDD compensation on the cross section. In addition, optical elements made of birefringence materials usually have dispersive properties different

from those of isotropic materials like BK7, which may not be suitable for use in such TPM system heavily relying on GDD compensation. Technically, these aspects of TPM system design specified to the un-tuned sub-10 fs pulse excitation are great challenges ahead of nonlinear optical microscopists.

Overall TPEF enhancements by the sub-10 fs TLP versus the 140 fs pulse excitation over the tuning range are noticeable, showing that the un-tuned sub-10 fs TLP excitation can effectively achieve TPEF enhancement despite the fact that its central wavelength may be detuned from the TPE spectrum peak position of a specific dye-molecule. In other words, fs-pulse central wavelength tuning is not necessarily the sole parameter for optimization of TPEF enhancement. The broadband un-tuned fs-pulse with its SH power spectrum appreciably overlapping TPE spectrum of a specific dye-molecule can be even more competent than narrowband fs-pulse tuning for TPEF enhancement, making itself as a convenient and effective excitation scheme without tuning. Generally, this way of plainly using broadband un-tuned fs-pulse excitation leads to differentiated TPEF enhancements among fluorescence dyes of choice, which highlights the frequency dependence of TPA cross section (or, overlap between fs-pulse SH power spectrum and dye-molecule TPE spectrum). The physics behind differentiated TPEF enhancements would suggest benefits and limitations of using broadband un-tuned fs-pulse excitation this way. With the broadband sub-10 fs TLP readily involved in both degenerate and non-degenerate TPA, this un-tuned ultrashort fs-pulse excitation simultaneously allows for more accessibility to TPA-associated final states and diversely promotes population of thus excited dye-molecules among the three dye-phantoms with

their distinct TPEF characteristics, leading to the differentiated TPEF enhancements. This good capability of broadband fs-pulse excitation for optimization of TPEF enhancement may be somewhat diminished with the dye-molecule TPE spectrum peak position falling off the fs-pulse SH power spectrum. Alternatively, selective excitation of multiple fluorescence probes by spectral tailoring of the broadband fs-pulse would achieve optimization of TPEF enhancement with greater flexibility and efficiency than conventional ways by narrowband fs-pulse tuning. This way of using the broadband fs-pulse spectrum could dynamically respond to each of the fluorescence labels *in situ* and accordingly achieve TPEF enhancement by manipulating coherence properties of broadband fs-pulse excitation *via* automation.

On the other hand, observations of the differentiated TPEF enhancements among the three single dye-phantoms suggest potential applications of broadband un-tuned fs-pulse excitation to optimization of multicolor TPEF enhancement, which is of practical significance since compromised excitations by narrowband fs-pulse tuning is not adequate to imaging tasks that requires high temporal and spectral resolutions. Owing to extensive overlap between the broadband fs-pulse SH power spectrum and the TPE spectra of the constituent dyes, the un-tuned sub-10 fs TLP best demonstrates its two-photon excitation capability by simultaneous excitation of the constituent dye-molecules in the mixture, achieving overall enhancement for better discernability of multicolor TPEF profiles and good detectability of multiple fluorescent probes *in situ*. Together with custom-designed multichannel spectral detection, simultaneous excitation with un-tuned broadband fs-pulse would optimally achieve multicolor TPEF enhancement in

multiple-dye labeled bio-samples, facilitate image processing, and help produce spectral cross-talk free images. It should be pointed out that optimization of TPEF enhancement has been broadly defined, which is under conceptual evolution throughout this research project, i.e., *from* TPEF enhancement based on the inverse proportionality law in narrowband fs-pulse regime *to* differentiated single-color TPEF enhancements by plainly using un-tuned broadband fs-pulse *to* selective excitation of multiple fluorescence labels by spectral tailoring and *to* simultaneous excitation for multicolor TPEF enhancement instead of compromise excitation by narrowband fs-pulse tuning. Essentially, optimization of TPEF enhancement concerns strategic utilization of un-tuned broadband fs-pulse for enhancing TPEF signals *in situ* of sufficiently high temporal and spectral resolutions without lowering the SBR of captured images at large imaging depths. In considering simultaneous excitation schemes with un-tuned broadband fs-pulse, a number of issues relevant to multicolor TPEF enhancement should be taken into account in order to make appropriate interpretations of biological significance from resultant multicolor TPEF signals. Environmental influences disturb fluorescence labels tagged to bio-samples in entangled ways, which complicates interpretations of resultant multicolor TPEF signals [49,51]. Clarification of associations between resultant multicolor TPEF signals and relevant environmental influences with phantom studies would be helpful. Simulations about OPA and solvent effects in the mixture explore methodology for such phantom studies and clarify difference between the measured multicolor TPEF profile and linear summation of single-color TPEF spectra. In practical imaging with TPM, OPA contribution to multicolor TPEF profile may be further complicated at large

imaging-depths where frequency dependent optical scattering in tissues would set in. Sometimes, entangled environmental influences on fluorescent probes could be so complicated that measured multicolor TPEF spectrum may give misleading information about distribution and localized concentrations of the probe-molecules, which makes appropriate interpretations difficult. Obviously, compromised excitation of multiple fluorescent probes by narrowband fs-pulse tuning would not be helpful to bettering discenability of multicolor TPEF profiles and detectability of constituent dye-molecules under environmental influences. Results of this proof-of-principle study on optimization of single- and multicolor TPEF enhancement with un-tuned broadband versus tunable narrowband fs-pulse excitation suggest possible ways of making improvements on the above-mentioned aspects. Expectedly, observations and conclusions made in this research project would be part of preliminary groundwork, being instructive to further considerations about optimization of TPEF enhancement by strategic utilization of broadband fs-pulse excitations for better performance of TPM.

REFERENCES

1. W. Denk, J. H. Strickler, and W. W. Webb, "Two-photon laser scanning fluorescence microscopy," Science **248**, 73-76 (1990).
2. W. R. Zipfel, R. M. Williams, and W. W. Webb, "Nonlinear magic: multiphoton microscopy in biosciences," Nat. Biotechnol. **21**, 1369-1377 (2003).
3. J. W. Lichtman and J. A. Conchello, "Fluorescence microscopy," Nat. Methods **2**, 910-919 (2005).
4. R. W. Boyd, *Nonlinear Optics*, 2nd Edition (Academic Press, 2003).
5. W. Koechner, *Solid-State Laser Engineering*, 6th Revised and Updated Edition (Springer, 2006).
6. T. Vo-Dinh, *Biomedical Photonics Handbook*, (CRC Press, 2003).
7. P. Theer and W, Denk, "On the fundamental imaging-depth limit in two-photon microscopy," J. Opt. Soc. Am. A **23**, 3139-3149 (2006).
8. T. Wilson, *Con-focal Microscopy*, (Academic Press, 1990).
9. C. Xu and W. W. Webb, "Measurement of two-photon excitation cross sections of molecular fluorophores with data from 690 to 1050nm," J. Opt. Soc. Am. B **13**, 481-491 (1996).
10. C. Xu, J. Guild, W. W. Webb, and W. Denk, "Determination of absolute two-photon excitation cross sections by *in situ* second-order autotocorrelation," Opt. Lett. **20**, 2372-2374 (1995).
11. R. Loudon, *The Quantum Theory of Light*, (Oxford, 1983).

12. M. Albota, D. Beljonne, J-L. Bredas, J. E. Ehrlich, J-Y. Fu, A. A. Heikal, S. E. Hess, T. Kogej, M. D. Levin, S. R. Marder, D. M-Maughon, J. W. Perry, H. Rockel, M. Rumi, G. Subramaniam, W. W. Webb, X-L. Wu, and C. Xu, "Design of organic molecules with large two-photon absorption cross sections," Science **281**, 1653-1656 (1998).
13. J. Zhang, R. E. Cambell, A. Y. Ting, and R. Y. Tsien, "Creating new fluorescent probes for cell biology," Nature Review, Mol. Cell Biol. **3**, 906-918 (2002).
14. N. C. Shaner, P. A. Steinbach, and R. Y. Tsient, "A guide to choose fluorescent proteins," Nat. Methods **2**, 905-909 (2005).
15. C. J. Bardeen, V. V. Yakovlev, J. A. Squier, K. R. Wilson, S. D. Carpenter, and P. M. Weber, "Effect of pulse shape on the efficiency of multiphoton processes: implications for biological microscopy," J. Biomedical Opt. **4**, 362-367 (1999).
16. R. A. Negres, J. M. Hales, A. Kobyakov, D. J. Hagan, and E. W. V. Stryland, "Two-photon spectroscopy and analysis with a white-light continuum probe," Opt. Lett. **27**, 270-272 (2002).
17. G. S. He, T-C Lin, and P. N. Prasad, "New technique for degenerate two-photon absorption spectral measurements using femtosecond continuum generation," Opt. Express **10**, 566-574 (2002).
18. X. Liang, W. Hu, and L. Fu, "Pulse compression in two-photon excitation fluorescence microscopy," Opt. Express **18**, 14893-14904 (2010).
19. D. Meshulach and Y. Silberberg, "Coherent quantum control of two-photon transition by a femtosecond laser pulse," Nature **396**, 239-242 (1998).

20. S. Tang, T. B. Krasieva, Z. Chen, G. Tempea, and B. J. Tromberg, "Effect of pulse duration on two-photon excited fluorescence and second harmonic generation in nonlinear optical microscopy," J. Biomedical Opt. **11**, 020501 (2006).

21. P. Xi, Y. Andegeko, L. R. Weisel, V. V. Lozovoy, and M. Dantus, "Greater signals, increased depth, and less photobleaching in two-photon microscopy with 10fs pulses," Opt. Commun. **281**, 1841-1849 (2008).

22. S. Pang, A. T. Yeh, C. Wang, and K. E. Meissner, "Beyond the $1/T_p$ limit: two-photon excited fluorescence using pulses as short as sub-10fs," J. Biomedical Opt. **14**, 054041 (2009).

23. D. Meshulach and Y. Silberberg, "Coherent quantum control of multiphoton transitions by shaped ultrashort optical pulses," Phys. Rev. A **60**, 1287-1292 (1999).

24. J-P Foing, M. Joffre, J-L Oudar, and D. Hulin, "Coherent effects in pump-probe experiments with chirped pump pulses," J. Opt. Soc. Am. B **10**, 1143-1148 (1993).

25. P. F. Moulton, "Spectroscopic and laser characteristics of Ti:Al_2O_3," J. Opt. Soc. Am. B **3**, 125-133 (1986).

26. A. M. Weiner, *Ultrafast Optics*, (John Wiley & Sons, Inc., 2009).

27. C. Rulliere, *Femtosecond Laser Pulses*, 2nd Edition (Springer, 2005).

28. A. V. Sokolov, L. M. Naveira, M. P. Poudel, J. Strohaber, C. S. Trendafilova, W. C. Buck, J. Wang, B. D. Strycker, C. Wang, H. Schuessler, A. Kolomenskii, and G. W. Kattawar, "Propagation of ultrashort laser pulses in water: linear absorption and onset of nonlinear spectral transformation," Applied Opt. **49**, 513-519 (2010).

29. R. Paschotta, *Encyclopedia of Laser Physics and Technology* (Wiley-VCH, 2008).

30. D. Kleckner, W. Marshall, M. J. A. de Dood, K. N. Dinyari, B-J Pors, W. T. M. Irvine, and D. Bouwmeester, "High finesse opto-mechanical cavity with a movable thirty-micron-size mirror," Phys. Rev. Lett. **96**, 173901/1-173901/4 (2006).

31. User Manual, *Dispersion Minimized Autocorrelator*, *FEMTOMETER*, FEMTOLASERS (1997-2007). www.femtolasers.com

32. B. Richards and E. Wolf, "Electromagnetic diffraction in optical systems. II. Structure of imaging field in an aplanatic system," Proc. Roy. Soc. London A **235**, 358-379 (1959).

33. C. J. R. Sheppard and H. J. Matthews, "Imaging in high-aperture optical system," J. Opt. Soc. Am. A **4**, 1354-1360 (1987).

34. F. A. Jenkins and H. E. White, *Fundamentals of Optics*, 4th Edition (McGraw-Hill, Inc., 1976).

35. R. Kingslake and R. B. Johnson, *Lens Design Fundamental*, 2nd Edition (Academic Press, Elsevier Inc., 2010).

36. Y. R. Shen, *The Principles of Nonlinear Optics*, (John Wiley & Sons., Inc., 1984).

37. T. N. Smirnova, E. A. Tikhonov, and M. T. Shpak, "Vibronic structure in the spectra of two-photon absorption of organic dye solutions," JETP Lett. **29**, 411-414 (1979).

38. H. Hashimoto, K. Isobe, A. Suda, F. Kannari, H. Kawano, H. Mizuno, A. Miyawaki, and K. Midorikawa, "Measurement of two-photon excitation spectra of fluorescence proteins with nonlinear Fourier-transform spectroscopy," Applied Opt. **49**, 3323-3329 (2010).

39. T. Brixner, N. H. Damrauer, P. Niklaus, and G. Gerber, "Photoselective adaptive

femtosecond quantum control in liquid phase," Nature **414**, 57-60 (2001).

40. V. V. Lozovoy and M. Dantus, "Systematic control of nonlinear optical processes using optimal shaped femtosecond pulses," Chem. Phys. Chem. **6**, 1971-2000 (2005).
41. J. P. Ogilvie, K. J. Kubarych, A. Alexandrou, and M. Joffre, "Fourier transform measurement of two-photon excitation spectra: applications to microscopy and optimal control," Opt. Lett. **30**, 911-913 (2005).
42. M. E. Dickinson, E. Simbuerger, B. Zimmermann, C. W. Waters, and S. E. Fraser, "Multiphoton excitation spectra in biological samples," J. Biomedical Opt. **8**, 329-338 (2003).
43. G. Labroile, R. S. Pillai, X. Solinas, C. Boudoux, N. Ogilvie, E. Beaurepair, and M. Joffre, "Dispersion-based pulse shaping for multiplexed two-photon fluorescence microscopy," Opt. Lett. **35**, 3444-3446 (2010).
44. R. Lansford, G. Bearman, and S. E. Fraser, "Resolution of multiple green fluorescence protein color variants and dyes using two-photon microscopy and imaging spectroscopy," J. Biomedical Opt. **6**, 311-318 (2001).
45. R. A. Neher, M. Mitkovski, F. Kirchhoff, E. Neher, and F. J. Theis, "Blind source separation techniques for the decomposition of multiply labeled fluorescence images," Biophy. J. **96**, 3791-3800 (2009).
46. C. Buehler, K. H. Kim, U. Greuter, N. Schlumpf, and P. T. C. So, "Single-photon counting multicolor fluorescence microscopy," J. Fluorescence **15**, 41-51 (2005).

47. A. M. Larson, A. Lee, P-F Lee, K. J. Bayless, and A. T. Yeh, "Ultrashort pulse, multispectral nonlinear optical microscopy," J. Innovative Opt. Health Sci. **2**, 27-35 (2009).

48. A. J. Raddosevich, M. B. Bouchard, S. A. Burgess, B. R. Chen, and E. M. C. Hillman, "Hyperspectral *in vivo* two-photon microscopy of intrinsic contrast," Opt. Lett. **33**, 2164-2166 (2008).

49. A. P. Demchenko, Y. Mely, G. Duportail, and A. S. Klymchenko, "Monitoring biophysical properties of lipid membranes by environmental-sensitive fluorescence probes," Biophy. J. **96**, 3461-3470 (2009).

50. A. Nag and D. Goswami, "Solvent effect on two-photon absorption and fluorescence of rhodamine dyes," J. Photochemistry and Photobiology A **206**, 188-197 (2009).

51. J. R. Lakowicz, *Principles of Fluorescence Spectroscopy*, 3rd Edition (Springer, 2006).

52. K. Vishwanath and M. A. Mycek, "Do fluorescence decay remitted from tissue accurately reflect intrinsic fluorescence lifetime?" Opt. Lett. **29**, 1512-1514 (2004).

53. M. Larson and A. T. Yeh, "*Ex vivo* characterization of sub-10-fs pulses," Opt. Lett. **31**, 1681-1683 (2006).

VITA

Name: Chao Wang

Address: Department of Biomedical Engineering,
5045 Emerging Technologies and Economic Development,
3120 TAMU, Texas A&M University,
College Station, Texas 77843-3120

Email Address: chaowang9@yahoo.com

Education: B.A., English, Xiamen University, 1984
M.S., Applied Physics, Shanghai Jiao Tong University, 1993
Ph.D., Biomedical Engineering, Texas A&M University, 2011